European Journal of Mechanical Engineering Research (EJMER)
Vol. 8, Issue 2, pp.42-85, 2021
Print ISSN: ISSN 2055-6551(Print)
Online ISSN: ISSN 2055-656X(Online)

NONLINEAR DYNAMICS INVESTIGATION OF CONTACT FORCE IN PLOYDYNE CAM AND FLAT-FACED FOLLOWER SYSTEM

Louay S. Yousuf
Assistant Professor, Department of Mechanical Engineering, San Diego State University, 5500 Campanile Drive, San Diego, CA, 92182-1323, USA

ABSTRACT: *Nonlinear dynamics behavior of contact force is investigated for different cam angular speeds (N) and different internal dimensions of the follower guide (F.G.I.D.). Largest Lyapunov exponent parameter conception is used to detect either the follower will detach from the cam or stays in permanent contact. Power spectrum analysis and Poincare' maps with phase-plane diagram are added to detect the non-periodic motion of the contact force. The follower is moved with three degrees of freedom. Multi degrees of freedom (spring-damper-mass) systems are added at the end of the follower stem to suppress the nonlinear dynamics behavior of the contact force of the follower. SolidWorks software is used in the numerical simulation of the contact force. Contact force and follower displacement are determined at different coefficient of restitution values. The friction and impact are considered between the cam and the follower and between the follower and its guide. The contact force is measured experimentally using OPTOTRACK/3020 by tracking the position of the follower through an infrared camera device. The value of contact force has declined with the increasing of cam angular speeds (N) and internal dimension of the follower guide (F.G.I.D.). The peak of nonlinear response of the follower displacement is reduced to (15 %, 32 %, 45 %, and 62 %) after using multi degrees of freedom system.*

Article Highlights

- *A multi degrees of freedom (spring-damper-mass) systems at the end of the follower stem are used to suppress the nonlinear dynamics phenomena of the contact force of the follower.*
- *The power density function with dominant frequency is calculated numerically for contact force and follower displacement using SolidWorks software.*
- *An OPTOTRAK / 3020 with an infrared camera device is used to track the follower position and measure the contact force experimentally.*
- *A phase-plane diagram with Poincare maps, Fast Fourier Transform (FFT), Lyapunov exponent conception are used to detect the non-periodic motion of the offset follower movement.*
- *Nonlinear dynamic response of the follower movement is investigated at different follower guides' internal dimensions (F.G.I.D.), cam angular velocities (N), and coefficient of restitution.*

KEYWORDS: nonlinear dynamics, lyapunov exponent, non-periodic motion, contact force.

ECRTD-UK: https://www.eajournals.org/
ULR: https://doi.org/10.37745/ejmer.2014

INTRODUCTION

The value of contact force between the cam and the follower is crucial which induces to either the follower will detach from the cam or stays in permanent contact. The application of this cam-follower system can be found in internal combustion engine. Sundar et al. used Hertzian contact theory to calculate the contact stiffness under both line and point contacts. They analyzed the coefficient of restitution model by using a single degree-of-freedom when the cam is rotating about a fixed pivot, [1]. Under the variation of cam rotational speed, Alzate et al. observed that the follower is detached from the cam and starts an emergence of periodic impacting behavior characterized by many impacts and chattering, [2]. Ciulli et al. measured the contact force experimentally during the rotation of a circular eccentric at different rotational speeds and preloads, [3]. Yousuf calculated the contact force against time for greasy and dry profile of the cam based on Hertzian contact pressure. He applied the theory of circular plate to calculate the bending deflection on the cam profile, [4]. The influence of maximum contact pressure of the bending deflection of the cam profile is studied for globoidal cam and roller follower system, [5]. Moreover, Yousuf, used Photoelastic technique to calculate the value of contact stress between the pear cam and roller follower mechanism. Four different position of the follower with the cam such as (0^o, 90^o, 180^o, and 270^o) degrees at different values of the compression load are considered, [6]. Pugliese et al. designed an apparatus to measure the contact force using an optical interferometry sensor and high speed camera. They showed different conditions of the contact at low and high magnification to detect the angular positions of the cam, [7]. Yang et al. extended a transient impact hypothesis of the contact model by considering the tangential slip between the cam and the follower. They showed that the cam and follower kept permanent contact when the cam rotational speed was low while the separation and oblique impact will happen at high speeds, [8]. The signal of follower motion in the y-direction has been processed depend upon data acquisition technique. Yousuf used Lyapunov exponent parameter and Fast Fourier Transform (FFT) analysis to detect the non-periodic motion of the follower at the contact point for different internal dimension of the follower guide and cam angular speeds, [9]. Non-periodic motion is examined using power spectrum analysis of Fast Fourier Transform (FFT) and phase plane diagram at the contact point between a polydyne cam and knife follower mechanism, [10]. Yousuf and Marghitu used largest Lyapunov exponent parameter to investigate the non-periodic motion in globoidal cam with roller follower system using different cam angular velocities and different internal dimensions of the follower guide, [11]. The main contribution of this work is to detect that either the follower will stay in permanent contact with the cam profile or there will be a separation between the cam and the follower. The aim of this paper, is to detect the nonlinear dynamics behavior of the contact force using the conception of largest Lyapunov exponent parameter, Power spectrum analysis and Poincare' maps at different follower guides internal dimensions (F.G.I.D.) and different cam angular velocities (N). The manuscript is organized as in below:

(a) In section (2), the analytic derivation of the general solution of follower displacement and contact force has been done using the theory of mechanical vibration. (b) In section (3), the numerical simulation of the follower displacement and contact force is done using SolidWorks

ECRTD-UK: https://www.eajournals.org/
ULR: https://doi.org/10.37745/ejmer.2014

software. (c) In section (4), the experiment test is carried out using OPTOTRAK 30/20 device to track the follower position and to calculate the contact force. (d) In section (5), the nonlinear dynamics tool is used to extract the time delay and the embedding dimensions of the follower displacement for the purpose of comparison. (e) in section (6), Wolf algorithm code is used to extract the value of largest Lyapunov exponent parameter. (f) In section (7), Fast Fourier Transform (FFT) is used to detect the periodic and non-periodic motion of the follower displacement and the contact force. (g) In section (8), the comparison of the contact force is made analytically, numerically and experimentally. (h) In section (9), average logarithmic divergence is applied on the set of follower displacement and contact force to determine the value of Lyapunov exponent. (i) In section (10), Poincare' maps with phase-plane diagram are used to detect the periodic and non-periodic motion of the contact force. (j) In section (11), the comparison of the follower displacement is made for one cycle of the cam rotation. (k) In section (12), the comparison of the present work with the previous publication is done using SolidWorks software. (l) In section (13), the multi degrees of freedom (spring-damper-mass) systems are used to suppress the nonlinear dynamics behavior of the contact force at the contact point.

Nonlinear Dynamic Response of the Follower

The equation of motion of cam-follower mechanism is as below:

$$\ddot{x} + 2\beta\dot{x} + \omega^2 x = F_1 + F_2 * \mathrm{Cos}(\Omega t) \quad (1)$$

Where:

$\frac{c}{m} = 2\beta$, $\frac{k}{m} = \omega^2, F_1 = k_1\Delta,\ F_2 = P_C$

The homogeneous solution of Equation (1) is:

$$x_H = e^{-\beta t}\left(C_1 * \mathrm{Sin}\left(\sqrt{(\omega^2 - \beta^2)}t\right) + C_2 * \mathrm{Cos}\left(\sqrt{(\omega^2 - \beta^2)}t\right)\right) \quad (2)$$

The particular solution of Equation (1) is:

$$x_P = G + A * \mathrm{Sin}(\Omega t) + B * \mathrm{Cos}(\Omega t) \quad (3)$$

Where: C_1, C_2, G, A, and B are constants.

The first and second derivatives of Equation (3) are:

$$\dot{x}_P = \Omega * A * \mathrm{Cos}(\Omega t) - \Omega * B * \mathrm{Sin}(\Omega t)$$

And;

$$\ddot{x}_P = -\Omega^2 * A * \mathrm{Sin}(\Omega t) - \Omega^2 * B * \mathrm{Cos}(\Omega t)$$

Substitute $(x_P, \dot{x}_P, \ddot{x}_P)$ into Equation (1) to obtain:

$$\omega^2 A - \Omega^2 A - 2\beta\Omega B)\mathrm{Sin}(\Omega t) + (\omega^2 B + 2\beta\Omega A - \Omega^2 B)\mathrm{Cos}(\Omega t) + G\omega^2 = F_1 + F_2\mathrm{Cos}(\Omega t) \quad (4)$$

Where:

$$A = \frac{2\beta\Omega F_2}{\omega^2 - \Omega^2 + 4\beta^2\Omega^2}$$

$$B = \frac{F_2}{\omega^2 - \Omega^2 + 4\beta^2\Omega^2}$$

$$G = \frac{F_1}{\omega^2}$$

ECRTD-UK: https://www.eajournals.org/
ULR: https://doi.org/10.37745/ejmer.2014

The general solution is:

$$x_C = x_H + x_P \quad (5)$$

Substitute the constant A, B, and G into Equation (3) and the homogeneous solution of Equation (2) into Equation (5) to obtain:

$$x_c = e^{-\beta t}\left(C_1 * \mathrm{Sin}\left(\sqrt{(\omega^2-\beta^2)}t\right) + C_2 * \mathrm{Cos}\left(\sqrt{(\omega^2-\beta^2)}t\right)\right) + \frac{F_1}{\omega^2} + \frac{2\beta\Omega F_2}{\omega^2-\Omega^2+4\beta^2\Omega^2}\mathrm{Sin}(\Omega t) + \frac{F_2}{\omega^2-\Omega^2+4\beta^2\Omega^2}\mathrm{Cos}(\Omega t) \quad (6)$$

The constants (C_1 and C_2) has been calculated from the boundary condition:

(1) at t = 0 and x = 0, (2) at t = 0 and $\dot{x} = 0$

After applying the boundary conditions on Equation (6) we obtain:

$$C_1 = \frac{\beta F_3}{\sqrt{\omega^2-\Omega^2}} - \frac{\Omega F_4}{\sqrt{\omega^2-\Omega^2}}$$

Where:

$$F_3 = \frac{(\omega^2-\Omega^2)F_1+4\beta^2\Omega^2F_1+\omega^2F_2}{\omega^2\Omega^2-4\beta^2\omega^2\Omega^2-\omega^4}$$

$$F_4 = \frac{2\beta\Omega F_2}{(\omega^2-\Omega^2)+4\beta^2\Omega^2}$$

$$C_2 = \frac{(\omega^2-\Omega^2)F_1+4\beta^2\Omega^2F_1+\omega^2F_2}{\omega^2\Omega^2-4\beta^2\omega^2\Omega^2-\omega^4}$$

The general solution of the follower displacement with offset is:

$$x_c = e^{-\beta t}\left(\frac{\beta\left(\frac{(\omega^2-\Omega^2)F_1+4\beta^2\Omega^2F_1+\omega^2F_2}{\omega^2\Omega^2-4\beta^2\omega^2\Omega^2-\omega^4}\right)-\frac{2\beta\Omega F_2}{(\omega^2-\Omega^2)+4\beta^2\Omega^2}}{\sqrt{\omega^2-\Omega^2}} * \mathrm{Sin}\left(\sqrt{(\omega^2-\beta^2)}t\right) + \frac{(\omega^2-\Omega^2)F_1+4\beta^2\Omega^2F_1+\omega^2F_2}{\omega^2\Omega^2-4\beta^2\omega^2\Omega^2-\omega^4} * \mathrm{Cos}\left(\sqrt{(\omega^2-\beta^2)}t\right)\right) + \frac{F_1}{\omega^2} + \frac{2\beta\Omega F_2}{\omega^2-\Omega^2+4\beta^2\Omega^2}\mathrm{Sin}(\Omega t) + \frac{F_2}{\omega^2-\Omega^2+4\beta^2\Omega^2}\mathrm{Cos}(\Omega t) \quad (7)$$

The spring with the elastic constant (k_1 = 38.0611 N/mm), and the preload extension (Delta = 37 mm), [12] is added between the installation table and the follower stem since it absorbs the energy of the spiral orbits of the follower movement. The normal force between the cam and the follower is illustrated in the following equation, [13]:

ECRTD-UK: https://www.eajournals.org/
ULR: https://doi.org/10.37745/ejmer.2014

$$P_C = \frac{1}{Cos(\emptyset)}[k_1(\Delta + x(t)) - kx(t) - c\dot{x}(t) - m\ddot{x}(t)] \quad (8)$$

Where:

$$\tan(\emptyset) = \frac{\dot{x}(t)}{x(t)+R_b^2} \quad [14]$$

Derive the general solution Eqn.(7) of the follower movement once and twice and substitute them into Eqn.(8) to obtain the analytic value of the contact force.

Numerical Simulation of Follower Displacement

SolidWorks software is used in the numerical simulation of the contact force and follower displacement, [15]. Four different internal dimensions of the follower guide such as (F.G.I.D. = 16, 17, 18, 19 mm) are used in which the clearance between the follower and its guide is a variable value. Impact is analyzed at the contact point based on different values of coefficient of restitution, while the friction is investigated using steel greasy and steel dry frictions. When the value of contact force is a maximum value which means that the cam and follower is in permanent contact. On the other hand when the value of contact force is zero which means that the follower will detach from the cam at high speeds. Figures (1) and (2) show the follower linear displacement mapping against time for (F.G.I.D. = 16 and 17 mm) and these figures indicate to how the follower detached from the cam profile at different cam angular velocities.

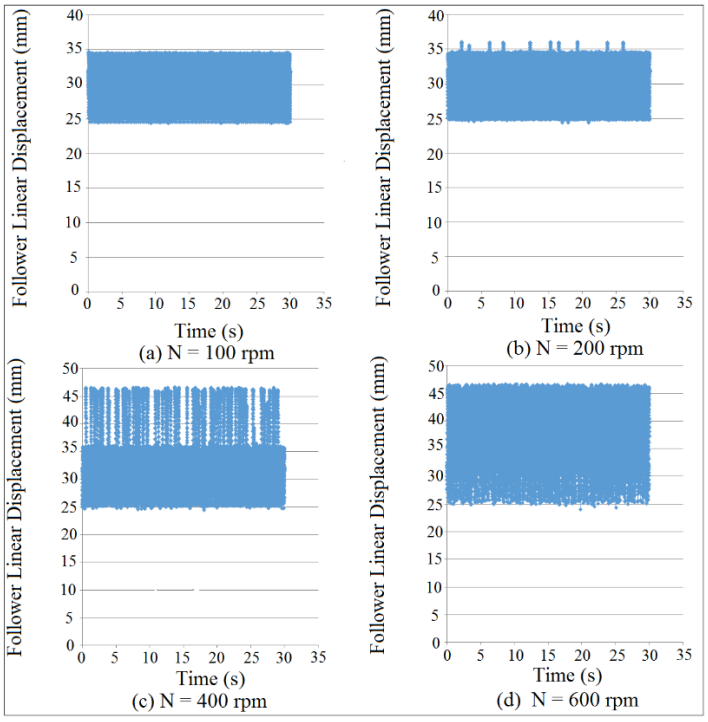

ECRTD-UK: https://www.eajournals.org/
ULR: https://doi.org/10.37745/ejmer.2014

Fig. 1 Follower linear displacement mapping against time for (F.G.I.D. = 16 mm).

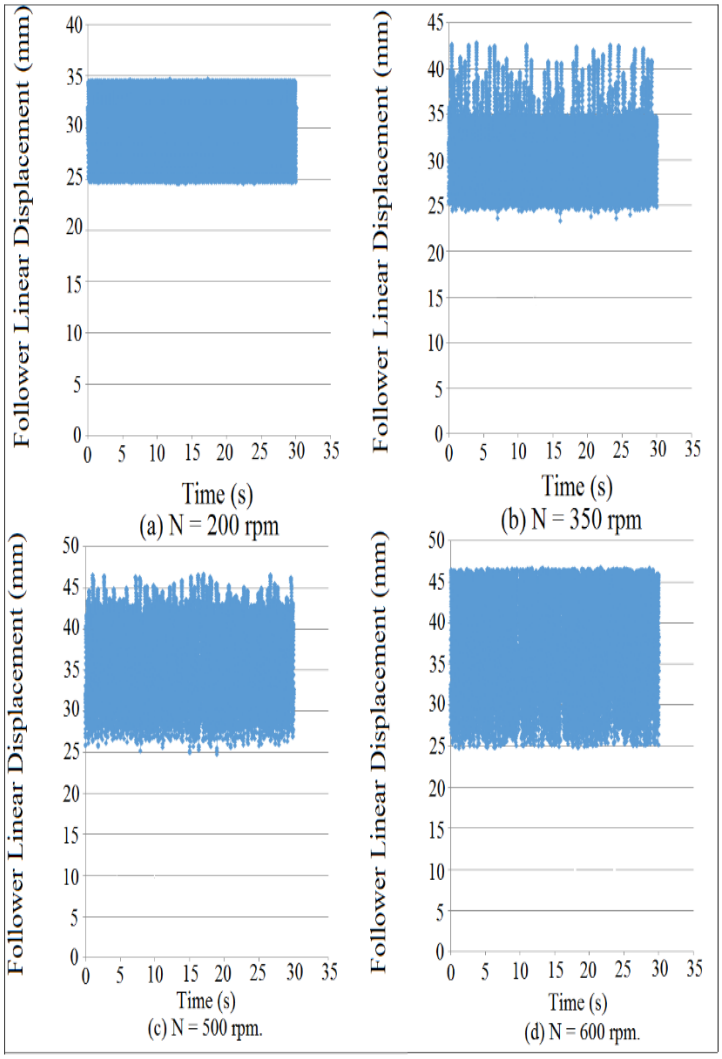

Fig. 2 Follower linear displacement mapping against time for (F.G.I.D. = 17 mm).

Figure (3) shows the follower displacement mapping against time at different coefficient of restitution values for (F.G.I.D. = 19 mm) and (N = 200 rpm). SolidWorks software is used in the simulation of follower displacement.

ECRTD-UK: https://www.eajournals.org/
ULR: https://doi.org/10.37745/ejmer.2014

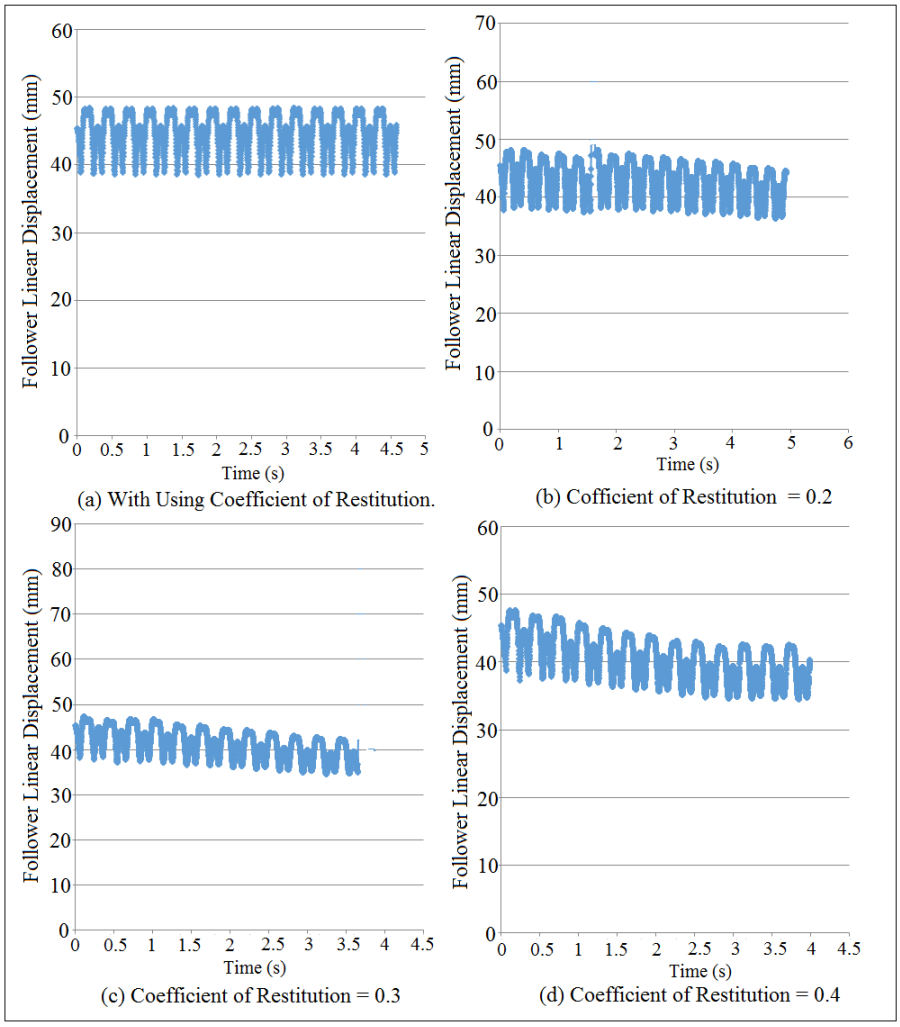

Fig. 3 Follower linear displacement mapping against time at different values of coefficient of restitution.

Experiment Test

An internal dimension of the follower guide (F.G.I.D. = 16 mm) with different angular velocity of the cam is used in the experiment test. A macro sensor through an infrared marker of OPTOTRAK / 3020 is used to capture the follower position. The follower is moved with three degrees of freedom in which the contact point is considered in the calculation. The macro sensor of a model number (DC750-5001), [16] is used to catch the signal of follower movement. The signal of follower movement is derived once and twice to determine follower acceleration. After multiplying the follower acceleration by the follower mass, it can be determined the contact force experimentally using Newton's second law of dynamic motion. Figure (4) shows the experiment test.

ECRTD-UK: https://www.eajournals.org/
ULR: https://doi.org/10.37745/ejmer.2014

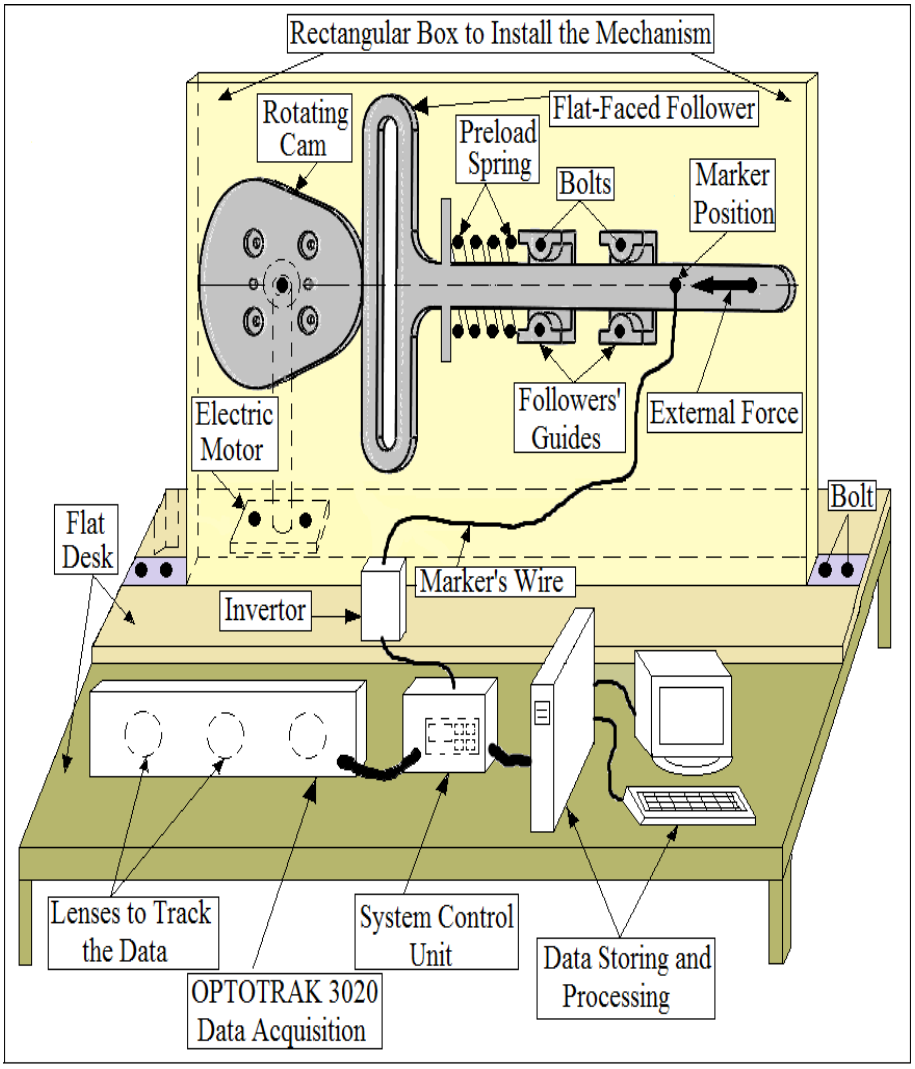

Fig. 4 Experiment test of cam-follower mechanism, [17].

Due to the interface feedback of an infrared 3-D camera of the OPTOTRAK / 3020 device, the follower movement is stocked in an excel file. The follower displacement is processed using MatLab software, [12].

Nonlinear Dynamics Tool

The algorithm of nonlinear dynamics tool is used to extract the values of time delay and embedding dimensions. The algorithm of average mutual information (AMI) and global false nearest neighbors (GFNN) are used to determine the time delay and the embedding dimensions respectively. The first minimum intersection point downward from (AMI) curve represents the time delay. Figures (5) and (6) show the comparison of time delay.

ECRTD-UK: https://www.eajournals.org/
ULR: https://doi.org/10.37745/ejmer.2014

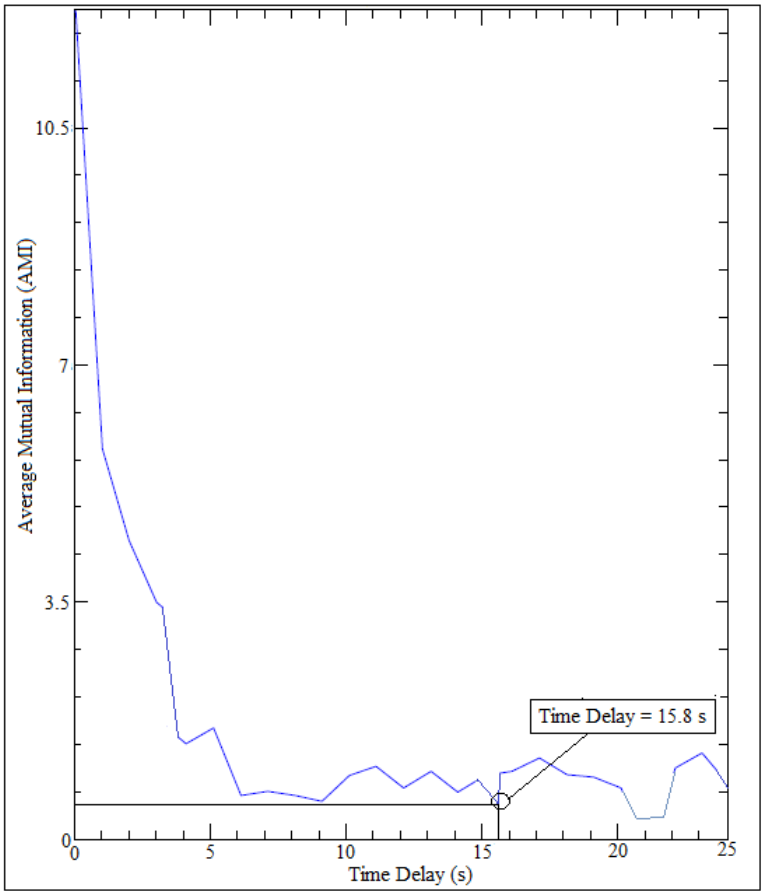

Fig. 5 Time delay of simulation analysis..

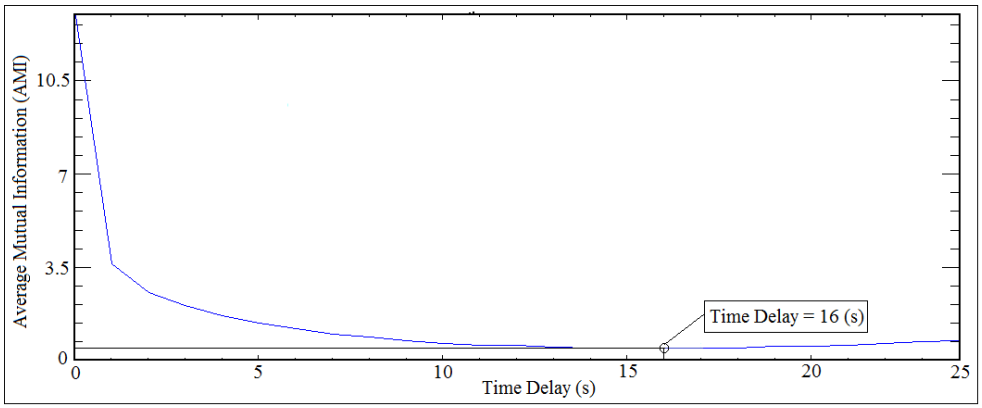

Fig. 6 Time delay of experiment test.

ECRTD-UK: https://www.eajournals.org/
ULR: https://doi.org/10.37745/ejmer.2014

When the global false nearest curve of the neighbors attractor reaches zero along way with the embedding dimensions which gives the value of embedding dimensions, [18]. One column of the contact force with time has been entered into nonlinear dynamic algorithm tool to quantify the values of time delay and embedding dimensions, [19]. Figures (7) and (8) show the comparison of embedding dimensions.

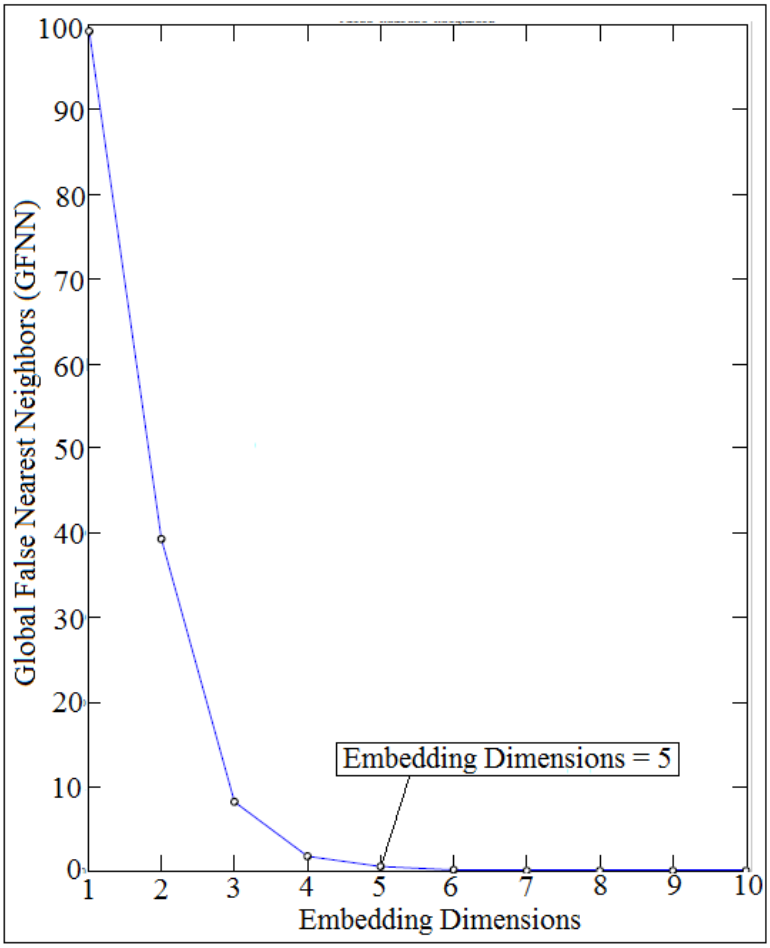

Fig. 7 Embedding dimensions of simulation analysis.

ECRTD-UK: https://www.eajournals.org/
ULR: https://doi.org/10.37745/ejmer.2014

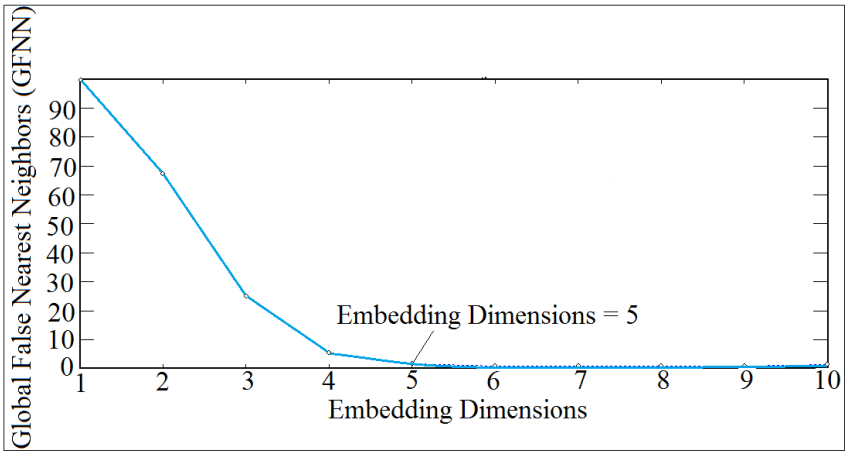

Fig. 8 Embedding dimensions of experiment test.

Largest Lyapunov Exponent Parameter

Largest Lyapunov exponent parameter is used to detect the detachment in cam-follower system through the contact force. When the value of Lyapunov exponent of the contact force is positive which means that there will be a detachment between the cam and the follower (contact force is zero). Negative largest Lapunov exponent value of the contact force indicates to periodic motion (the cam and the follower is in permanent contact) and the contact force has a maximum value. Wolf algorithm code based on MatLab software is used to extract the values of largest Lyapunov exponent by monitoring the orbital divergence, [20]. Equations (9) and (10) are used to build Wolf algorithm code of dynamic tool, [21].

$$d(t) = De^{\lambda t} \quad (9)$$

$$y(i) = \frac{1}{\Delta t}[\ln d_j(i)] \quad (10)$$

A four and ten strides of times are selected which gives a best fit of linear slopes of average logarithmic divergence of largest Lyapunov exponent. Figure (9) shows the numerical value of largest Lyapunov exponent against number of samples at (F.G.I.D. = 16 mm) and (N = 400 rpm). All the values of Lyapunov exponent parameter is taken at their respective equilibrium point. One column of the contact force with the use of time delay and embedding dimension values are used in Wolf algorithm to extract the numerical value of largest Lyapunov exponent parameter. One column of the contact force has been taken from SolidWorks software and used in the dynamic tool of Wolf algorithm program.

ECRTD-UK: https://www.eajournals.org/
ULR: https://doi.org/10.37745/ejmer.2014

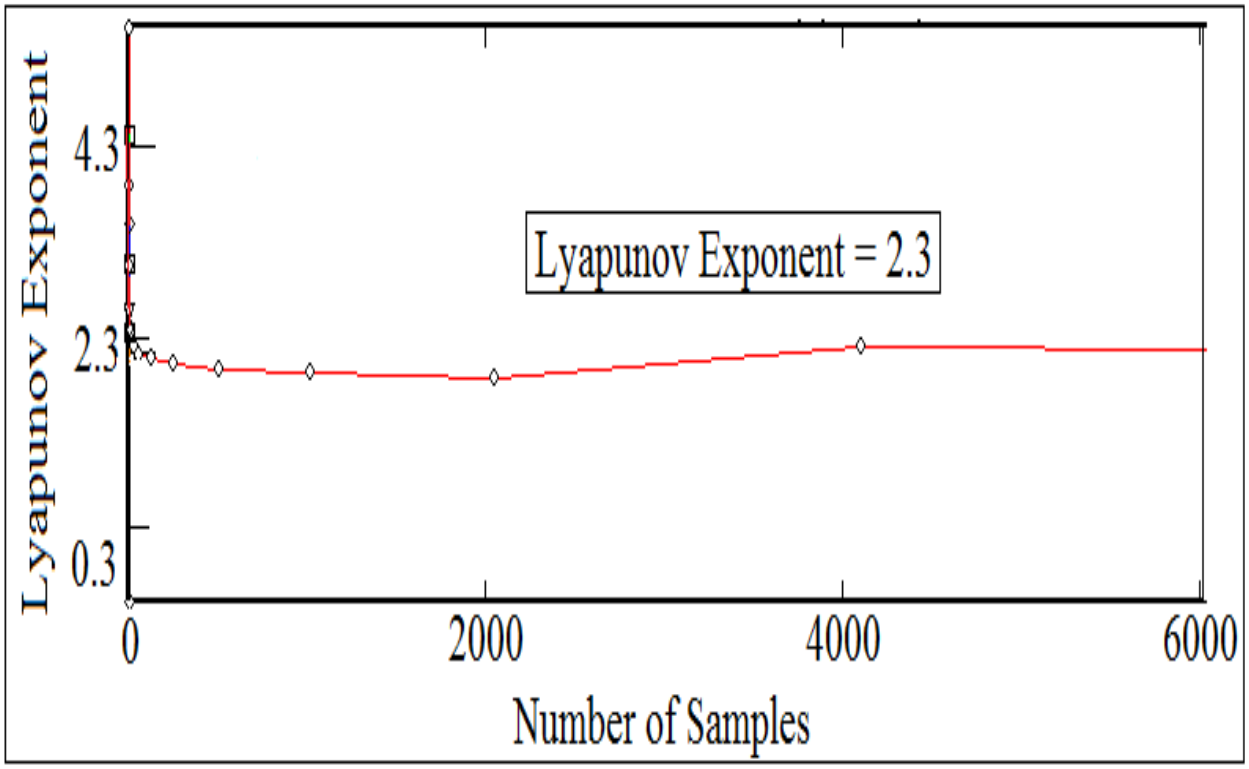

Fig. 9 Local Lyapunov exponent against number of samples for (F.G.I.D. = 16 mm) and (N = 400 rpm).

Fast Fourier Transform (FFT)

Power spectrum analysis gives six frequencies peaks' alongside with the fundamental frequency. The first peak in power spectrum tool refers to fundamental frequency (F), [22]. The amplitude of fundamental frequency and the other frequencies' peaks indicate to periodic motion (the contact force has a maximum value and the cam and the follower is in permanent contact). When the frequencies' peaks have been started disappearing from (FFT) diagram, the motion is non-periodic (contact force is approaching zero and the detachment between the cam and the follower has been occurred). Figures (10) and (11) show the comparison of power spectrum analysis of Fast Fourier Transform (FFT) at (F.G.I.D. = 17 mm) and (N = 200 rpm). The numerical simulation values of the contact force is calculated using SolidWorks software and after that the one column of contact force is treated using (FFT). The experiment data of the follower displacement is tracked using OPTOTRAK 30/20 device and Newton's second law of dynamic motion is applied based on the values of follower mass and acceleration to determine one column of the contact force. One column of the contact force is treated using (FFT).

ECRTD-UK: https://www.eajournals.org/
ULR: https://doi.org/10.37745/ejmer.2014

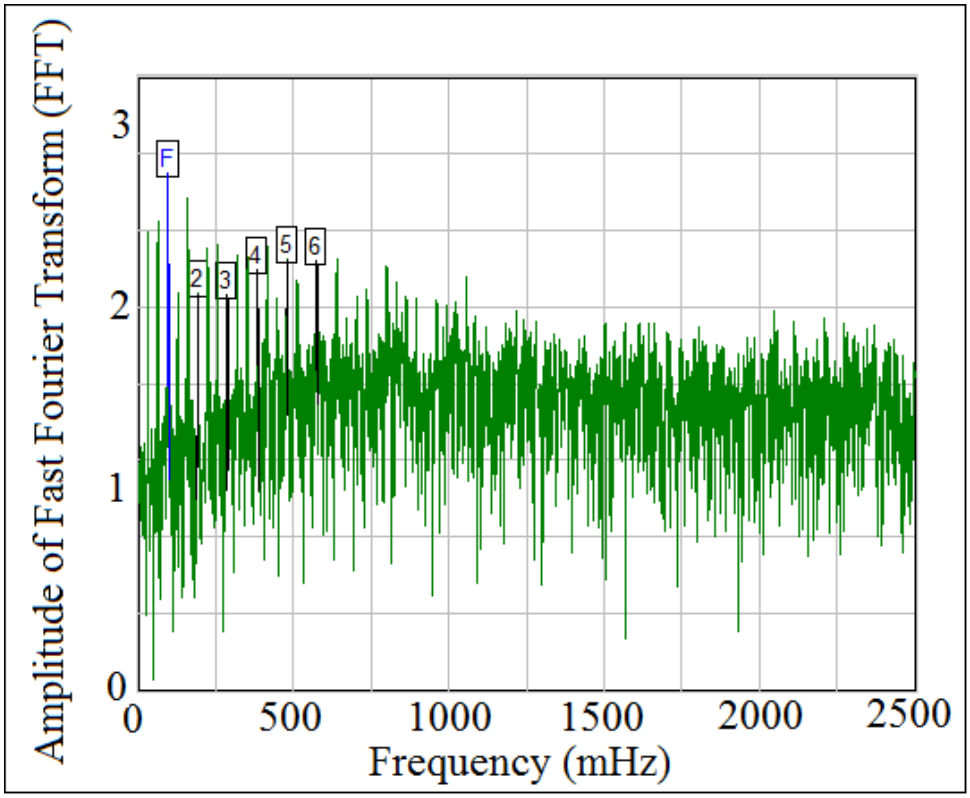

Fig. 10 Power spectrum analysis of the experiment test.

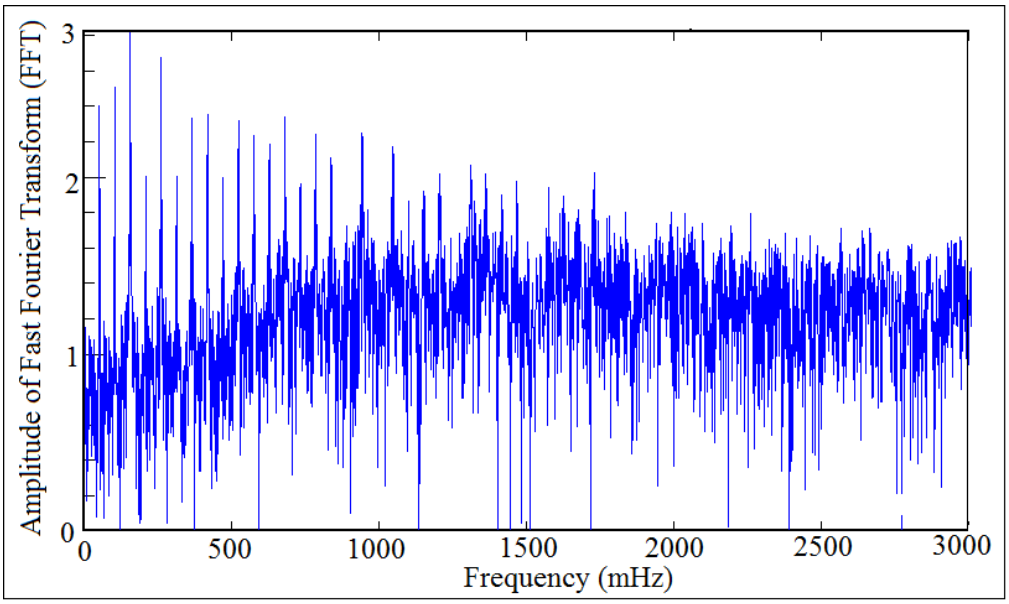

Fig. 11 Power spectrum analysis of the numerical simulation.

ECRTD-UK: https://www.eajournals.org/
ULR: https://doi.org/10.37745/ejmer.2014

The dominant frequency is occurred due to high speeds of the cam and due to the residual vibration in the follower. There is no dominant frequency at low speeds of the cam and when the cam and the follower are both in permanent contact. The energy of the follower stem needs to be dissipated due to friction and impact since this will get rid of the dominant frequency. Figure (12) shows the power density function with the dominant frequency of Fast Fourier Transform (FFT) at (F.G.I.D. = 17 mm) and (N = 200 rpm) for contact force and follower displacement. SolidWorks software is used in the numerical simulation of the dominant frequency for both the contact force and the follower displacement.

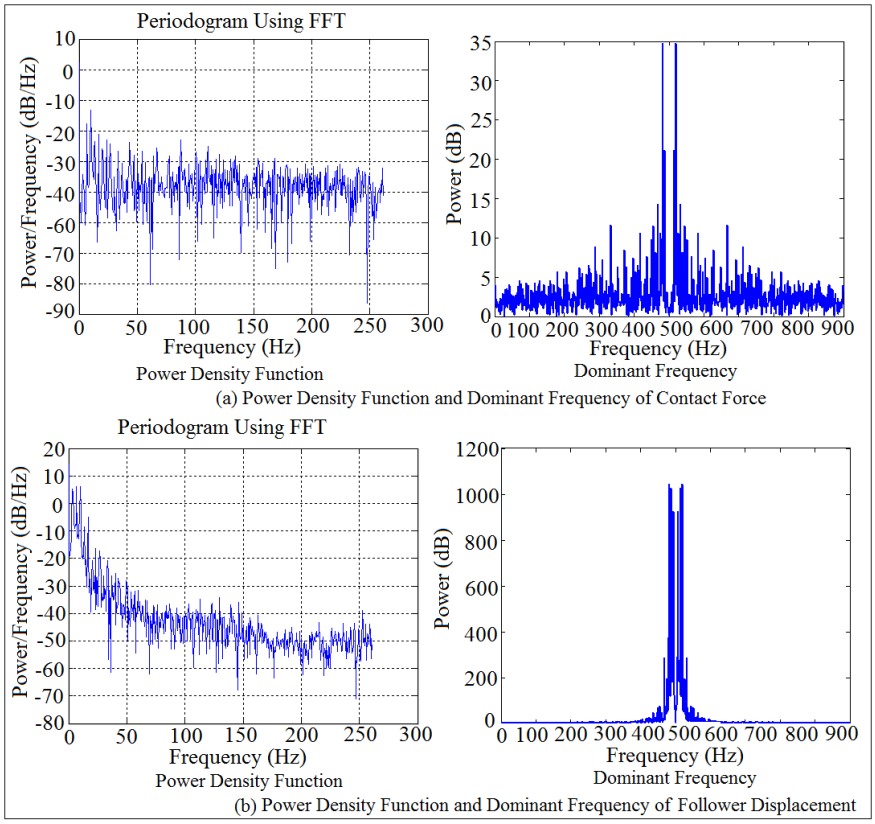

Fig. 12 Power density function and dominant frequency for (F.G.I.D. = 17 mm) and (N = 200 rpm).

Contact Force in Mechanical Systems

The weight of the follower is sufficient to maintain the contact since the follower is moved with simple harmonic motion. Also, the preload spring between the installation table and the follower stem must be properly designed to maintain the contact. In this paper, the follower stem is designed to be constrained by two guides due to follower movement with three degrees of freedom. Figures (13) and (14) show the mapping of contact force against time for internal dimension of the follower guide (F.G.I.D. = 16 and 17 mm) at different cam angular velocities. SolidWorks software is used in the calculation of contact force at different (F.G.I.D.) and (N).

ECRTD-UK: https://www.eajournals.org/
ULR: https://doi.org/10.37745/ejmer.2014

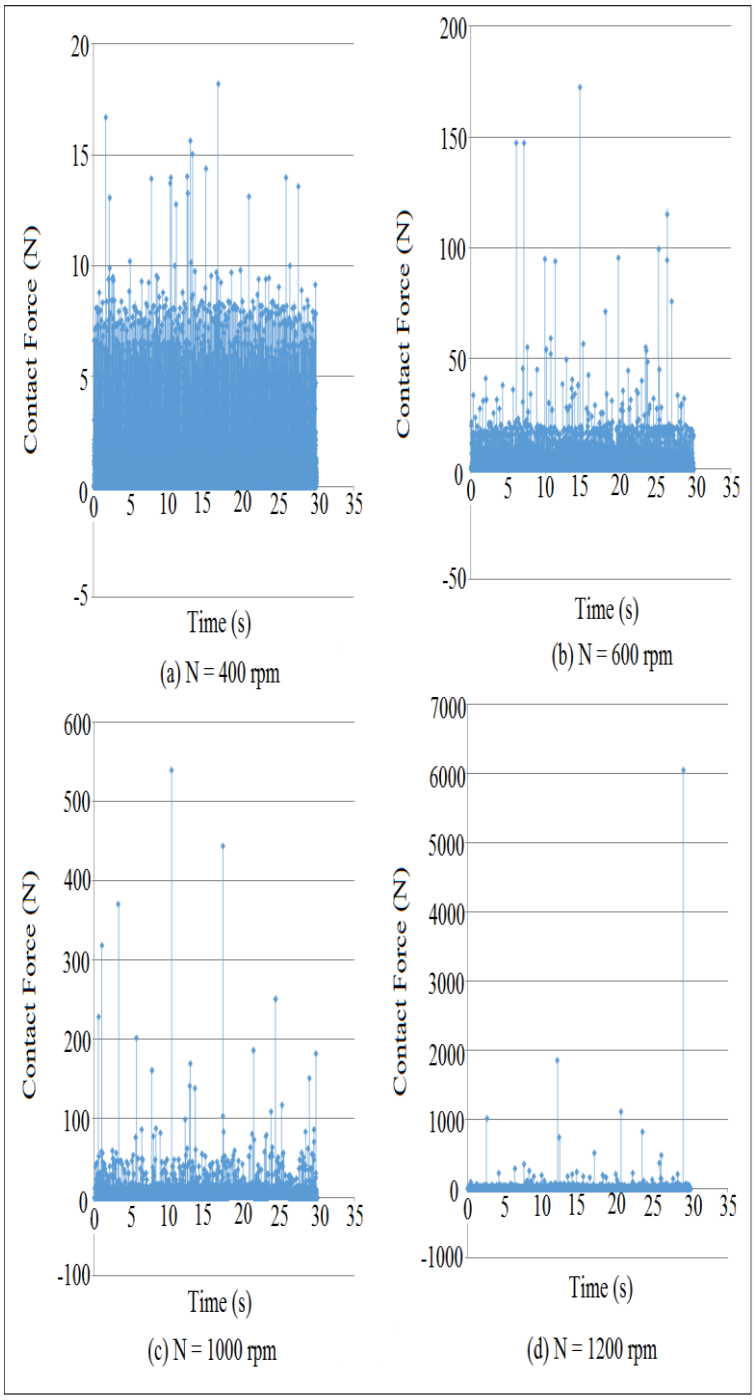

Fig. 13 Contact force mapping against time at different cam angular velocities for (F.G.I.D. = 16 mm).

ECRTD-UK: https://www.eajournals.org/
ULR: https://doi.org/10.37745/ejmer.2014

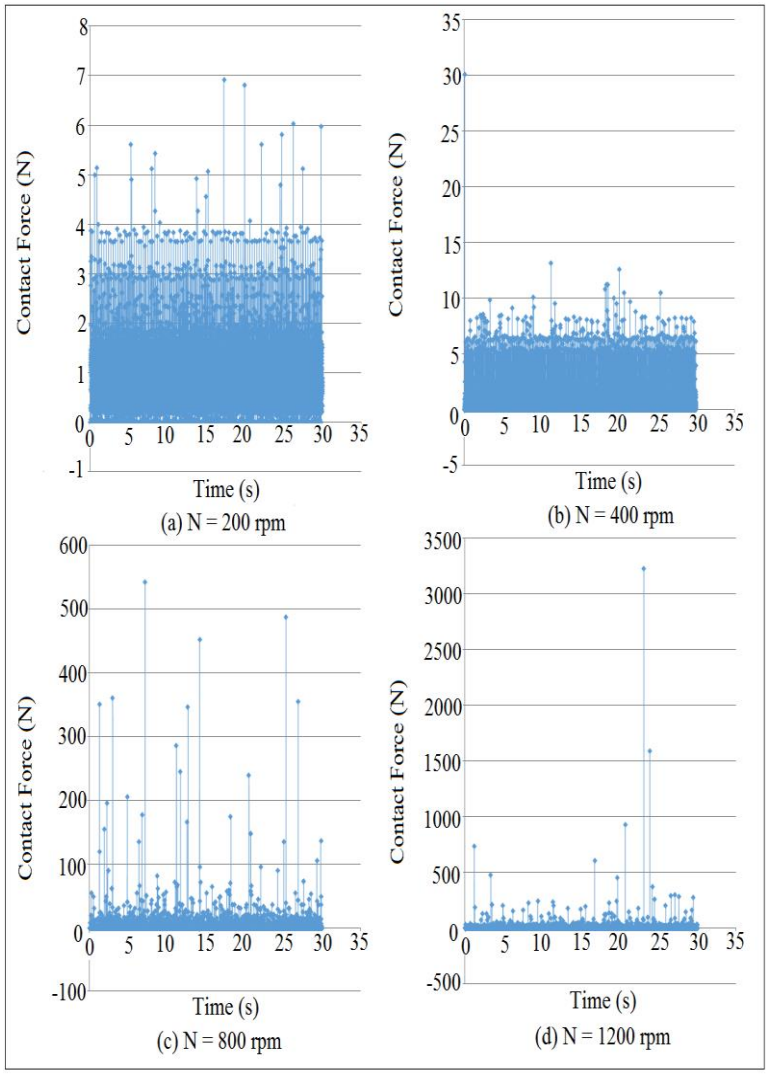

Fig. 14 Contact force mapping against time at different cam angular velocities for (F.G.I.D. = 17 mm).

Figure (15) shows the comparison of the contact force against time at (F.G.I.D. = 16 mm) and (N = 400 mm). The analytic set of data of the contact force is calculated after applying eqn.(8), while the numerical simulation of the contact force is determined using SolidWoks software. The experimental set of data of the contact force is calculated after tracking the follower position using OPTOTRAK 30/20 device and applying Newton's second law of dynamic motion based on the follower mass and follower acceleration as mentioned in (Experiment Test) section.

ECRTD-UK: https://www.eajournals.org/
ULR: https://doi.org/10.37745/ejmer.2014

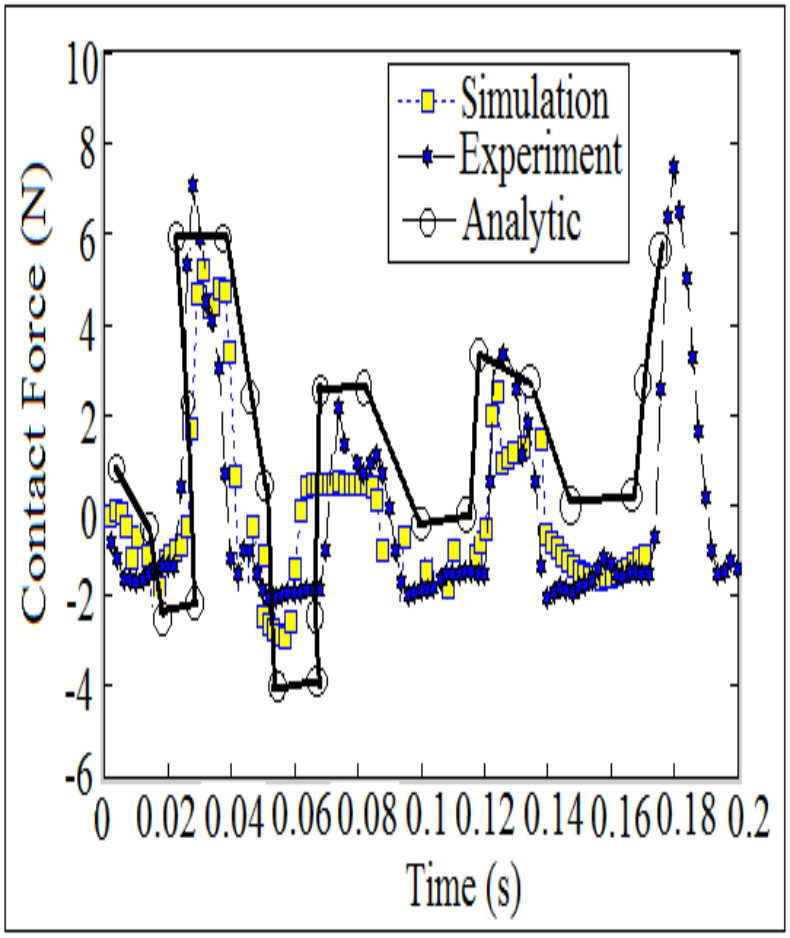

Fig. 15 Comparison of contact force against time.

Average Logarithmic Divergence of Contact Force

Average logarithmic divergence is used to extract the largest Lyapunov exponent parameter value for the contact force. The straight line represents the slope of average logarithmic divergence which reflects the value of Lyapunov exponent parameter. The curve represents the logarithm function against time of the contact force. As known, that the logarithm function treats any set of data by a straight line which gives the value of largest Lyapunov exponent. Figure (16) shows the comparison of average logarithmic divergence of contact force against time for (F.G.I.D. = 16 mm) and (N = 200 rpm) respectively to extract the value of Lyapunov exponent. The analytic set of data of the contact force is calculated after applying eqn.(8), while the numerical simulation of the contact force is determined using SolidWoks software. The experimental set of data of the contact force is calculated after tracking the follower position using OPTOTRAK 30/20 device and applying Newton's second law of dynamic motion based on the follower mass and follower acceleration as mentioned in (Experiment Test) section.

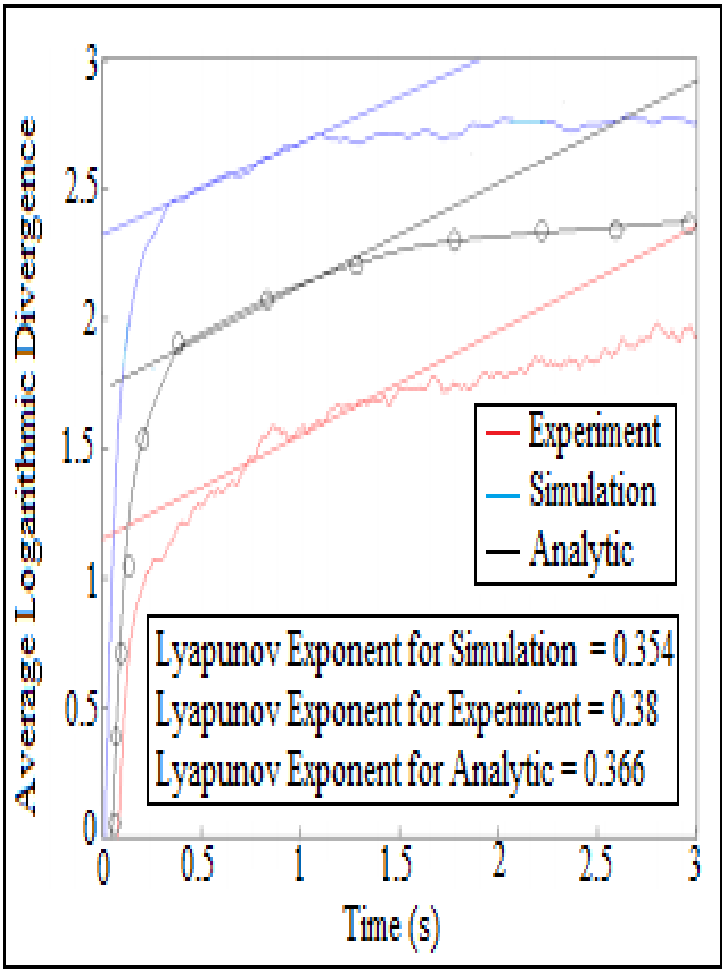

Fig. 16 Average logarithmic divergence against the time for (F.G.I.D. = 16 mm) and (N = 200 rpm).

Poincare' Map

Poincare' maps is used to investigate the periodicity of contact force diagram. Poincare' map represents records of the contact status between the cam and the follower. It is useful in identifying either the follower is detached due to high speeds or stays in permanent contact with the cam, [23]. The results of Poincare' maps are done at different internal dimensions of the follower guide (F.G.I.D.) and different cam angular velocities (N). Figures (17) and (18) show the mapping of Poincare' maps for (F.G.I.D. = 16 and 18 mm) and different cam angular speeds (N). SolidWorks software is used in the simulation of Poincare maps.

ECRTD-UK: https://www.eajournals.org/
ULR: https://doi.org/10.37745/ejmer.2014

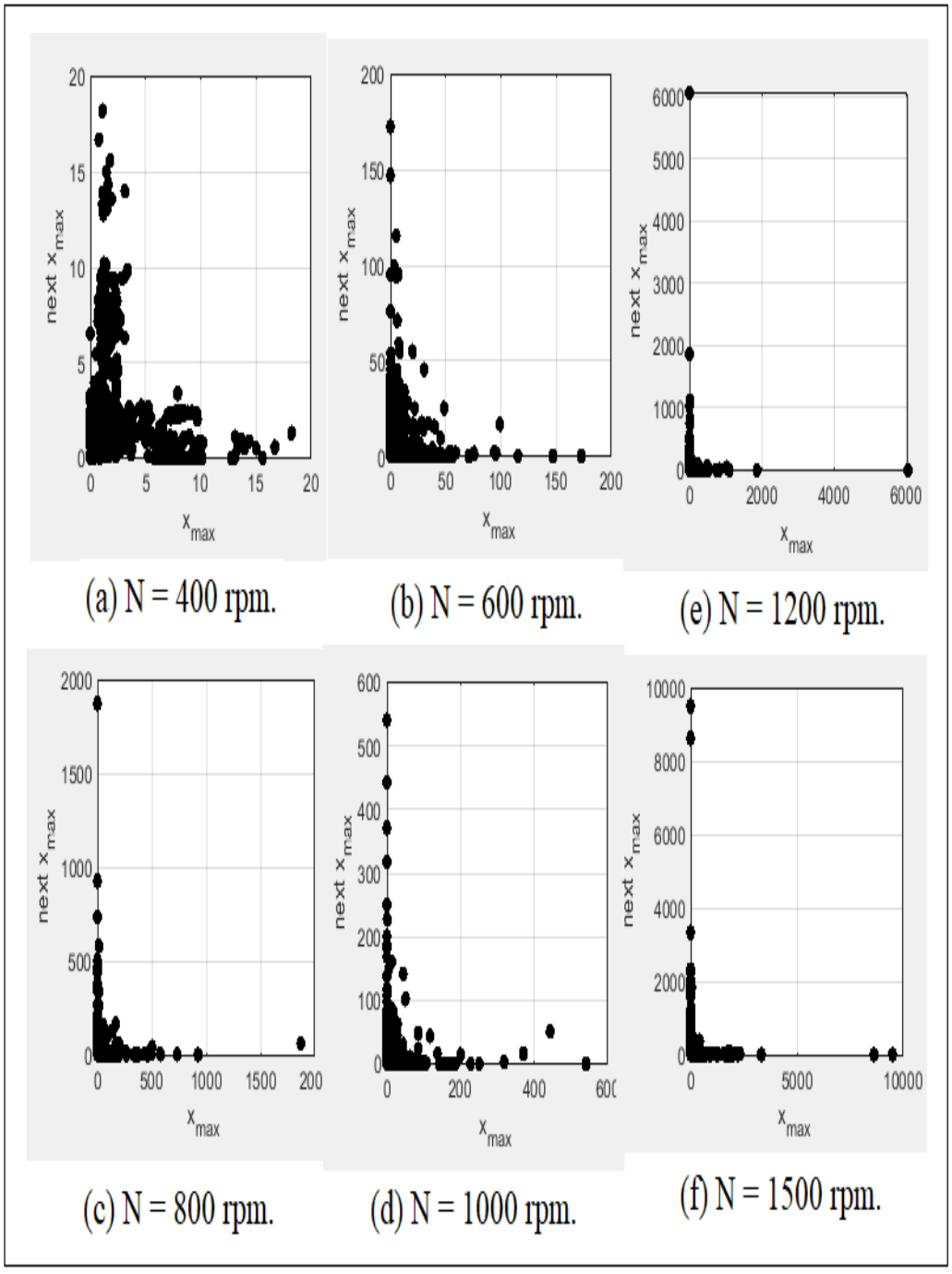

Fig. 17 Poincare' maps for (F.G.I.D. = 16 mm) at different cam angular speeds.

ECRTD-UK: https://www.eajournals.org/
ULR: https://doi.org/10.37745/ejmer.2014

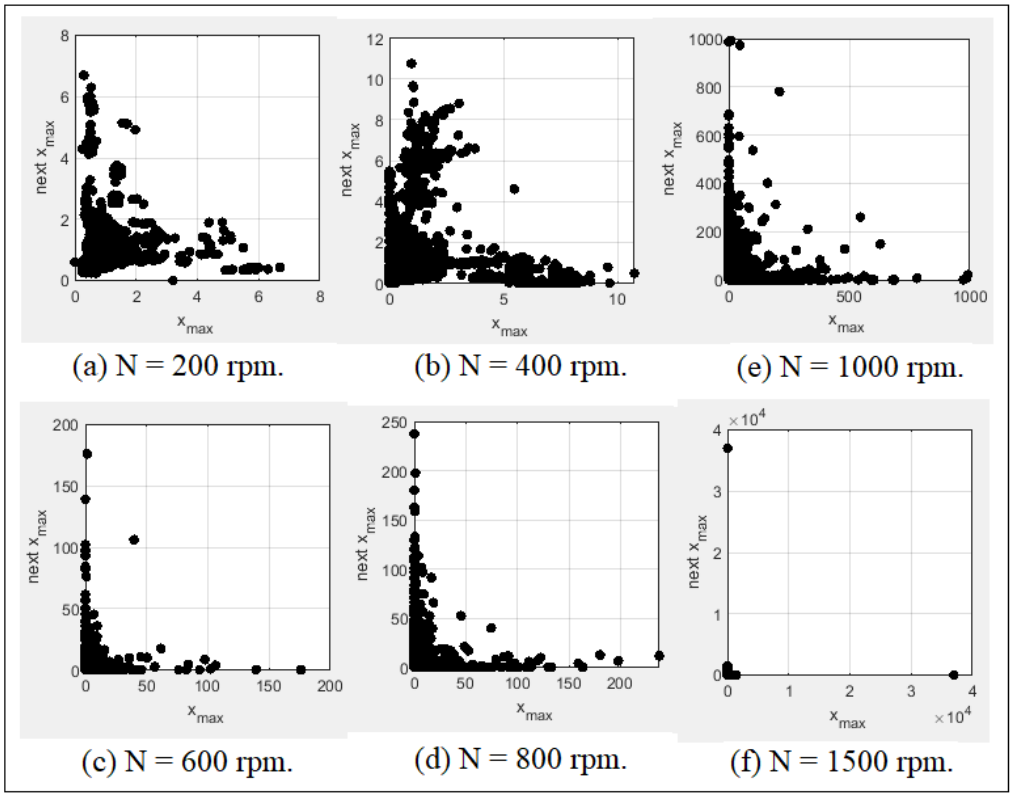

Fig. 18 Poincare' maps for (F.G.I.D. = 18 mm) at different cam angular speeds.

Phase-plane diagram works alongside with Poincare' map to check for periodic and non-periodic motion of the follower movement. When the orbit of the follower movement is one closed curve which indicates to periodic motion while when the orbit of the follower movement diverges with no limits of spiral open cycles which gives indication to non-periodic motion and chaos. Figure (19) shows the mapping of phase-plane diagram after using different values of coefficient of restitution at (F.G.I.D. = 19 mm) and (N = 200 rpm). The broken lines in the upper and lower surfaces in phase-plane diagram indicates to multi impacts inside one cycle of the cam rotation as illustrated in Figs. (19b, 19c, 19d). The broken lines in the upper and lower surfaces in the phase-plane diagram is increased with the increasing of coefficient of restitution values. The variation of the follower movement is increased with the increasing of coefficient of restitution values. Figure (19a) shows smooth contact between the cam and the follower at low speed (N = 200 rpm) without the use of coefficient of restitution parameter in which there is no broken lines in the upper and lower surfaces in the phase-plane diagram. SolidWorks software is used in the simulation mapping of phase-plane diagram.

ECRTD-UK: https://www.eajournals.org/
ULR: https://doi.org/10.37745/ejmer.2014

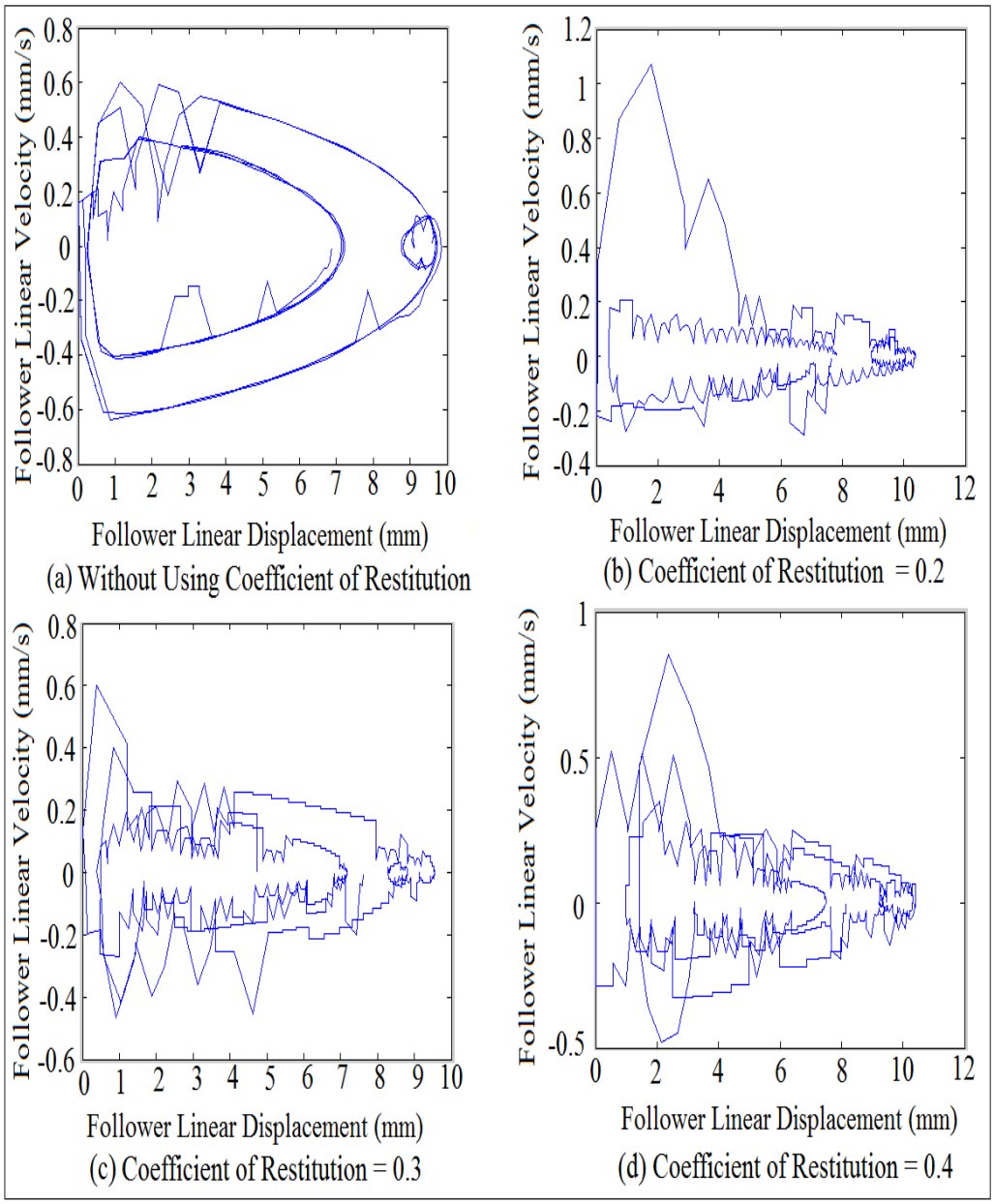

Fig. 19 Phase-plane diagram mapping using different values of coefficient of restitution.

Follower Displacement Verification

In this paper, the cam profile with return-dwell-rise-dwell-return-dwell-rise-dwell is selected, [24]. The follower displacement is shown in Fig. (20) for one cycle of cam rotation when the follower at (F.G.I.D. = 16 mm) and (N = 300 rpm).

ECRTD-UK: https://www.eajournals.org/
ULR: https://doi.org/10.37745/ejmer.2014

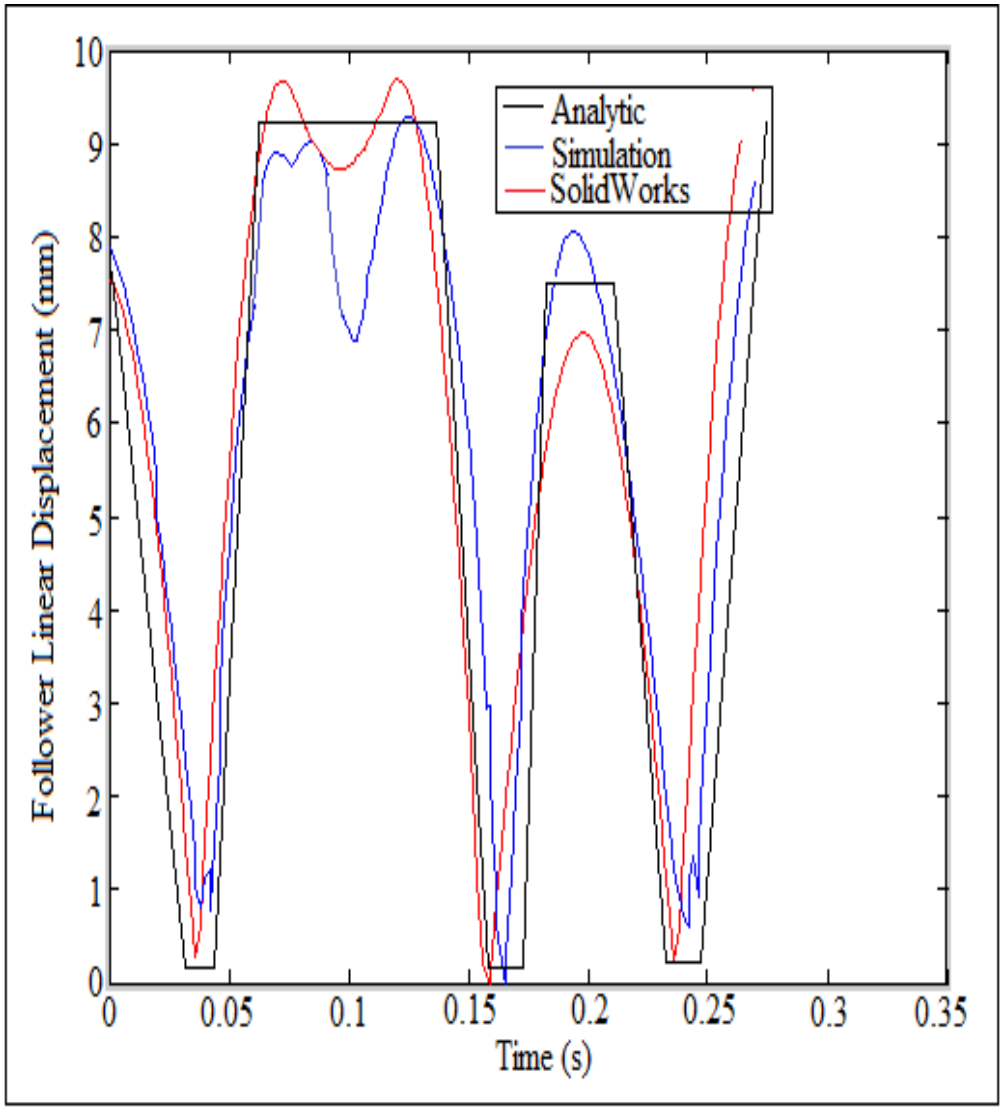

Fig. 20 Comparison of follower linear displacement.

The analytic follower displacement is done by applying Eqn.(7). Follower linear displacement is tracked experimentally using the optical sensor mounted on the follower through a 3-D lenses camera in the OPTOTRAK /3020 device. Solidworks software is used in the numerical simulation of follower linear displacement.

Comparison of Present Work With the Previous Publications

Figure (21) shows the comparison of nonlinear response of the follower against time. In the present work, the system with (F.G.I.D. = 17 mm) and (N = 200 rpm) is considered in the simulation without linkage mechanism. Ref.[19] is claimed that the follower is connected to linkage mechanism. The comparison of follower displacement is done using SolidWorks software.

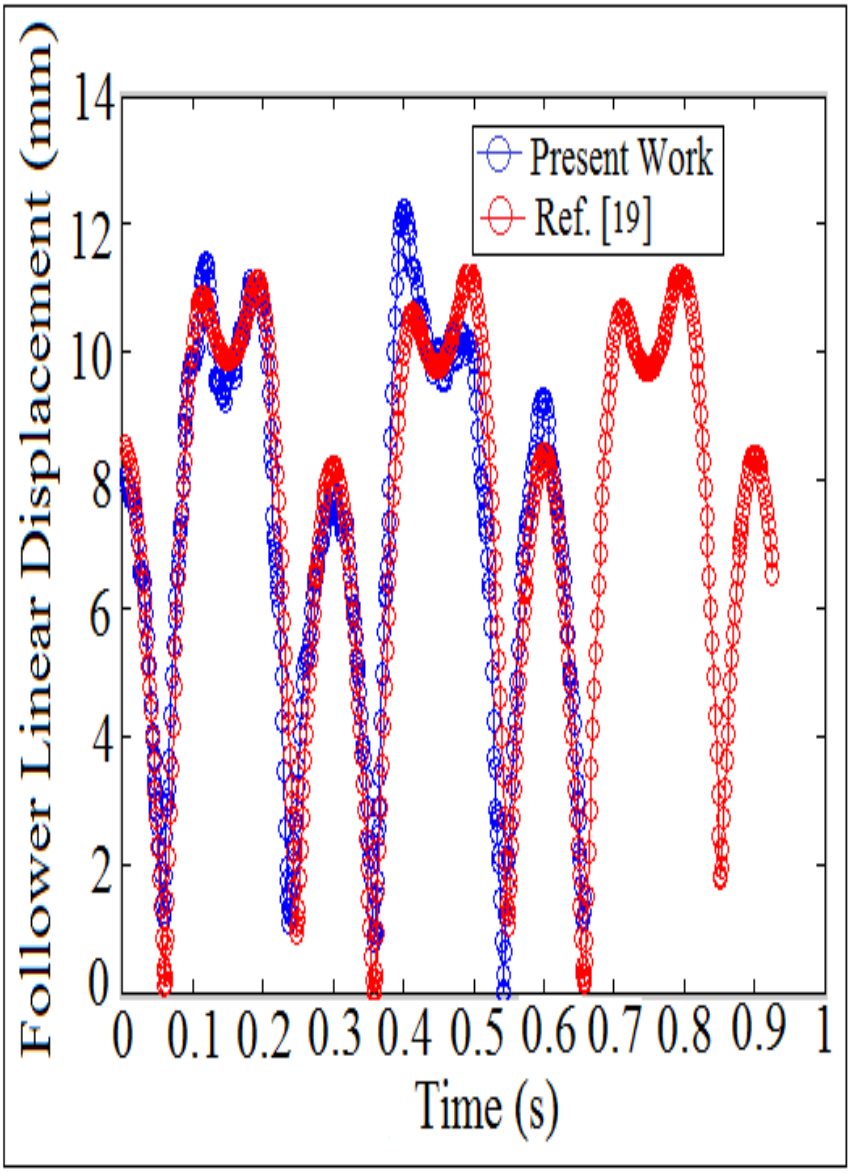

Fig. 21 Comparison of nonlinear response of the follower with and without connection to linkage mechanism.

Multi Degrees of Freedom of System

A multi degrees of freedom (spring-damper-mass) systems are added at the end of follower stem to suppress the nonlinear dynamics phenomena of the follower movement. All the springs and viscous damping coefficients have the same values in which ($k_1 = k_2 = k_3 = k_4 = 7$ N/mm), and the viscous damping coefficient ($c_1 = c_2 = c_3 = c_4 = 0.875$ N.s/mm). The spring with the elastic constants such as spring index ($C_{index} = 7$), coil diameter (d = 2.5 mm), outside diameter (OD = 20 mm), number of turn (n = 10) and (length = 25 mm), [12] is selected since it absorbs the energy of

ECRTD-UK: https://www.eajournals.org/
ULR: https://doi.org/10.37745/ejmer.2014

the spiral orbits of the follower movement. Figure (22) shows the multi degrees of freedom system. SolidWorks is used in the numerical simulation of phase-plane diagram of multi degree of freedom systems.

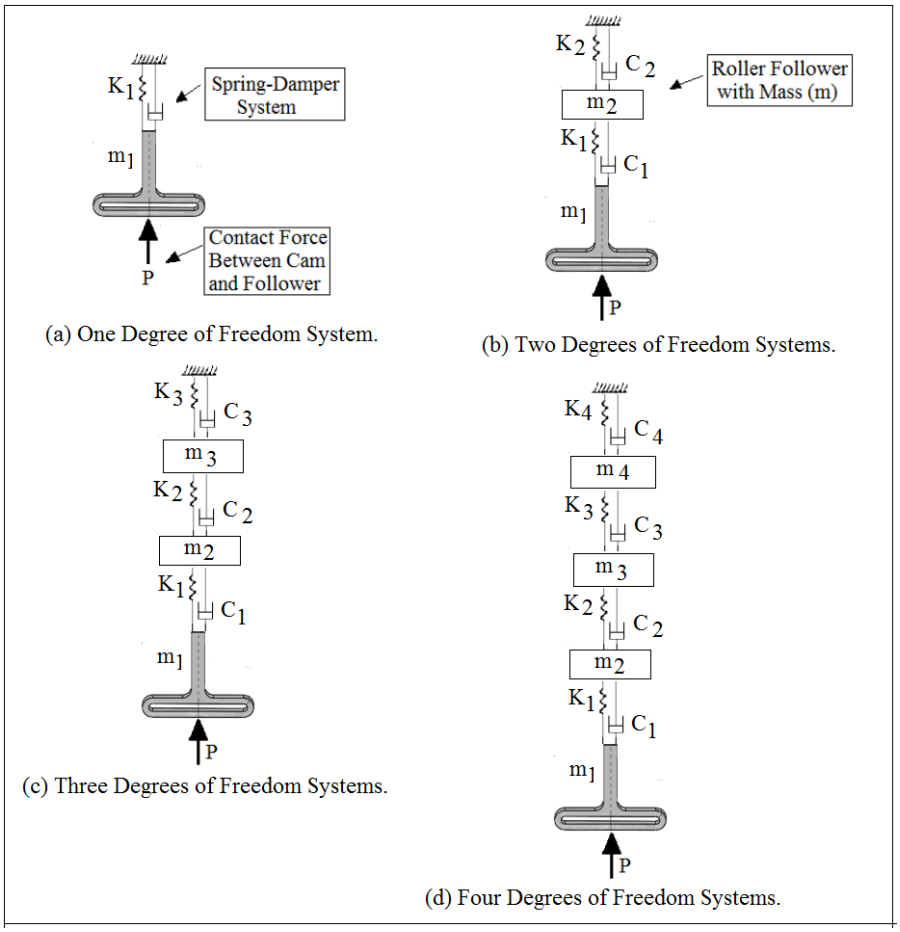

Fig. 22 Multi degrees of freedom system.

Figure (23) show the follower linear displacement against time at (F.G.I.D. = 17 mm) and (N = 300 rpm) using multi degrees of freedom systems. Multi degrees of freedom (spring-damper-mass) system is used to decrease the amplitude of follower linear displacement against time. The amplitude of follower linear displacement is reduced to (15 %, 32 %, 45 %, and 62 %) for one, two, three, and four degrees of freedom systems respectively. SolidWorks software is used in the numerical simulation of linear displacement using multi degree of freedom systems.

ECRTD-UK: https://www.eajournals.org/
ULR: https://doi.org/10.37745/ejmer.2014

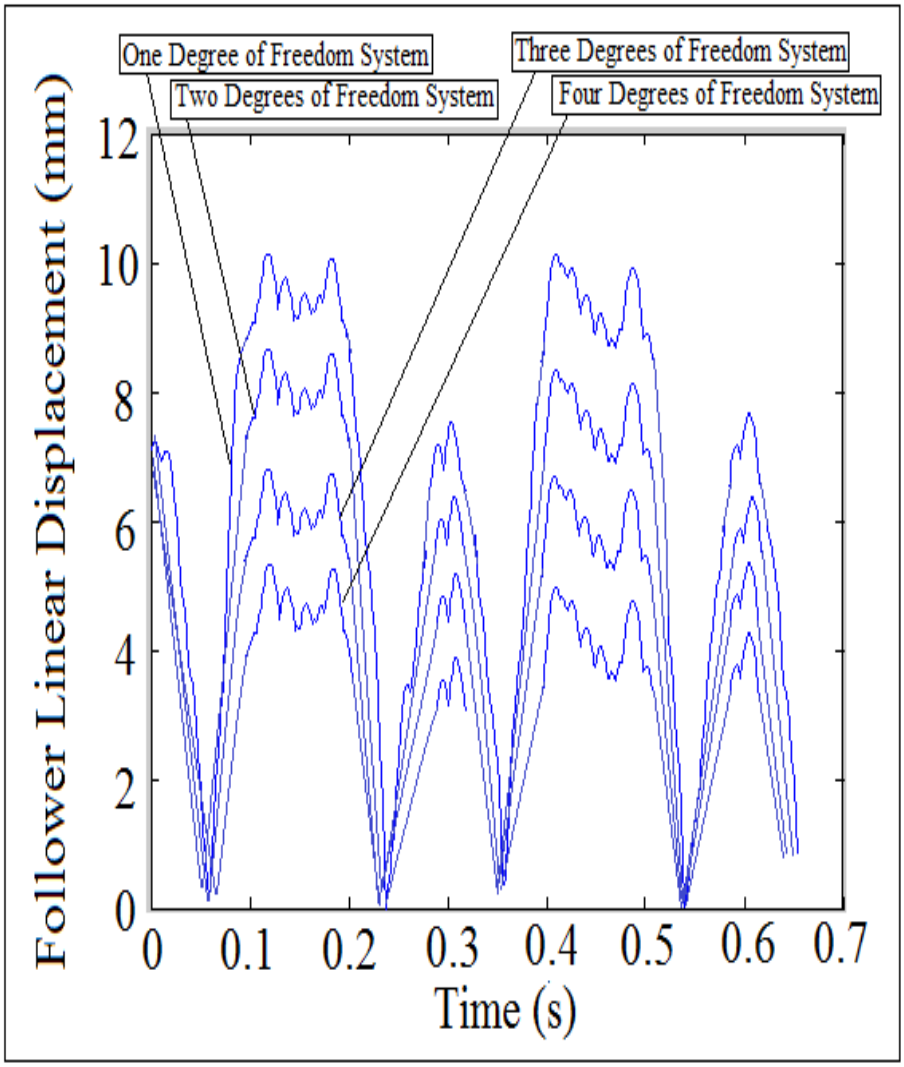

Fig. 23 Follower linear displacement against time at (F.G.I.D. = 17 mm) and (N = 300 rpm) using multi degrees of freedom systems.

RESULTS AND DISCUSSIONS

Figures (24) and (25) show the mapping of follower linear displacement against time at different cam angular velocities for (F.G.I.D. = 18 and 19 mm) respectively. There is no detachment between the cam and the follower as indicated in Figs. (24a) and (25a) which means that the contact force has a maximum value. The detachment between the cam and the follower is increased with the increasing of cam angular velocities which means that the contact force is approaching zero, as illustrated in Figs. (24b, 24c, 24d) and (25b, 25c, 25d). SolidWorks is used in the simulation.

ECRTD-UK: https://www.eajournals.org/
ULR: https://doi.org/10.37745/ejmer.2014

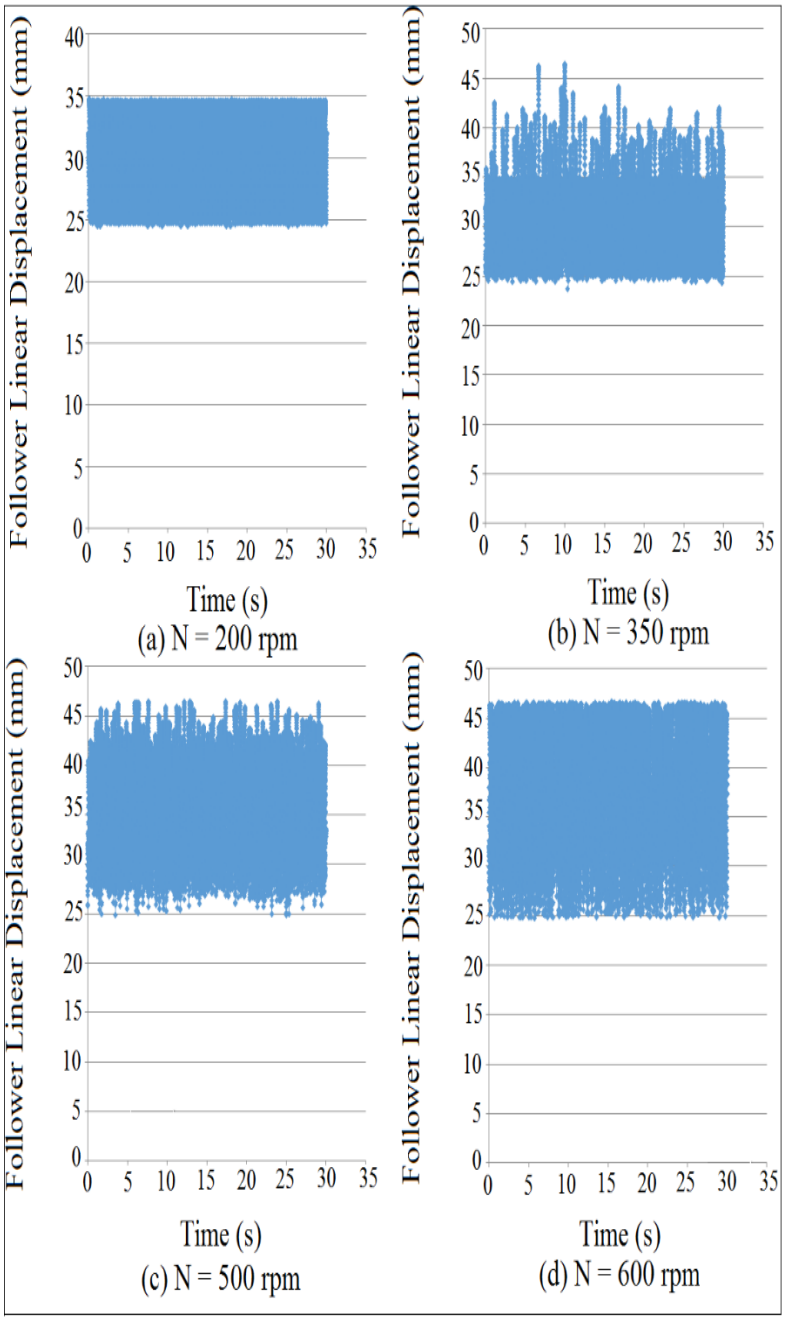

Fig. 24 Follower linear displacement mapping against time for (F.G.I.D. = 18 mm).

ECRTD-UK: https://www.eajournals.org/
ULR: https://doi.org/10.37745/ejmer.2014

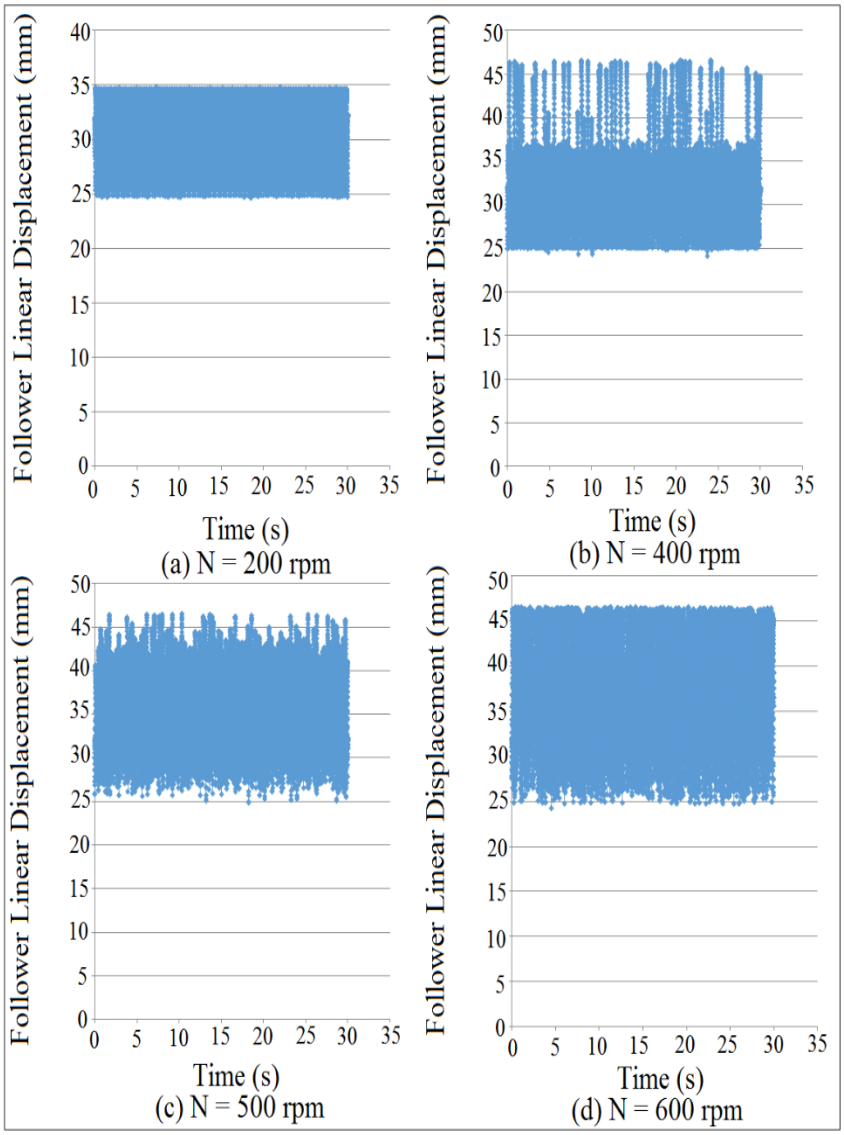

Fig. 25 Follower linear displacement mapping against time for (F.G.I.D. = 19 mm).

Figures (26) and (27) show the mapping of contact force at different cam angular velocities (N) and different internal dimensions of the follower guide (F.G.I.D.). The nonlinear dynamics behavior of the contact force is quasi-periodic as shown in Figs. (26a) and (27a), while the non-periodic of the contact force is illustrated in Figs. (26b, 26c, 26d) and (27b, 27c, 27d). The value of contact force has declined with the increasing of cam angular velocities and internal dimensions of the follower guide. The system with (F.G.I.D. = 18 mm) and (N =1500 rpm) has a minimum value of contact force (separation between the cam and the follower will occur). SolidWorks is used in the simulation.

ECRTD-UK: https://www.eajournals.org/
ULR: https://doi.org/10.37745/ejmer.2014

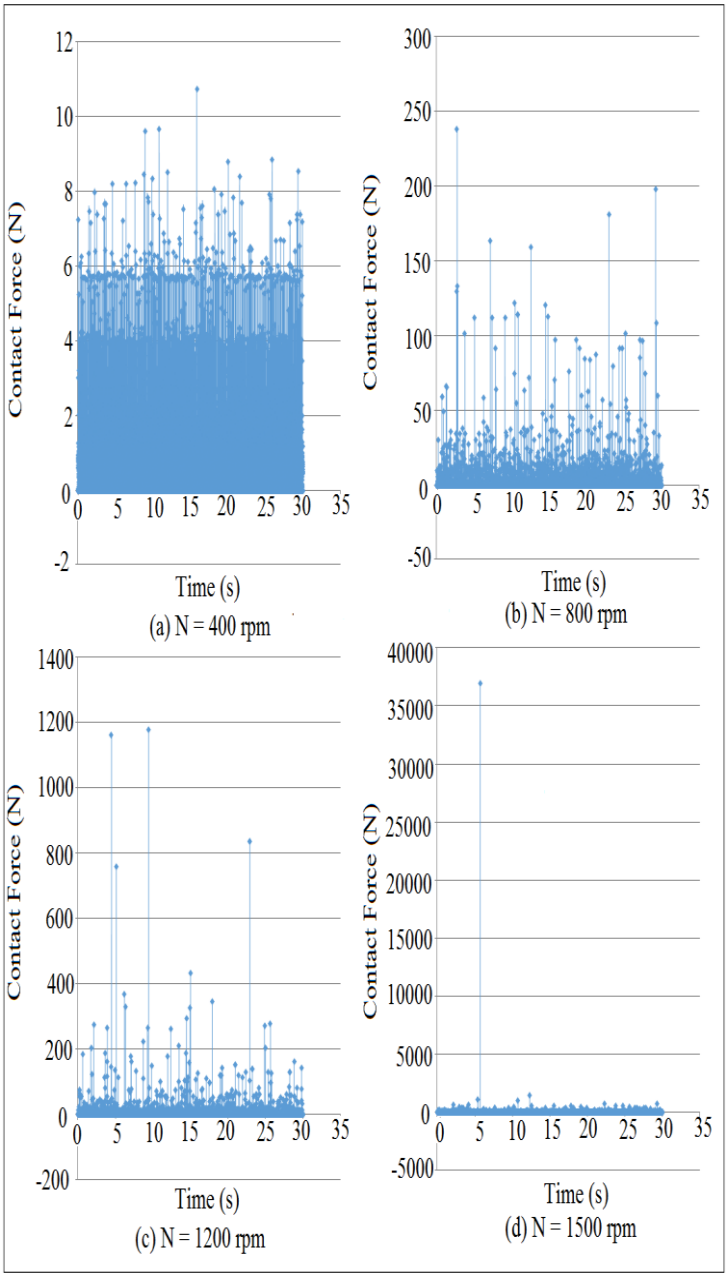

Fig. 26 Contact force mapping against time for (F.G.I.D. = 18 mm).

ECRTD-UK: https://www.eajournals.org/
ULR: https://doi.org/10.37745/ejmer.2014

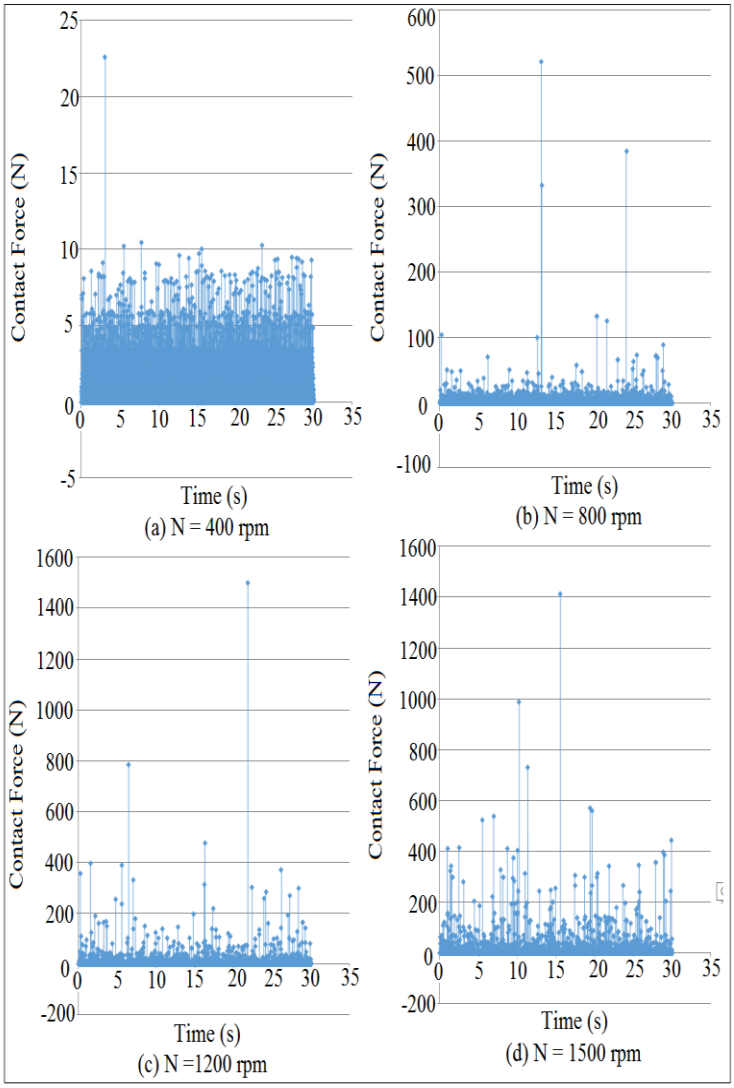

Fig. 27 Contact force mapping against time for (F.G.I.D. = 19 mm).

Figure (28) shows the maximum detachment height of the follower against cam angular velocities at different internal dimension of the follower guide. The maximum detachment height of the follower is increased with the increasing of cam angular velocities. The detachment height of the follower is in a minimum value at (N = 200-300 rpm) for (F.G.I.D. = 16, 17, and 18 mm). There is no detachment between the cam and the follower at (N = 100-200~rpm) for all internal dimensions of the follower guide which means that the contact force has a maximum value (no separation between the cam and the follower will occur). SolidWorks is used in the simulation.

ECRTD-UK: https://www.eajournals.org/
ULR: https://doi.org/10.37745/ejmer.2014

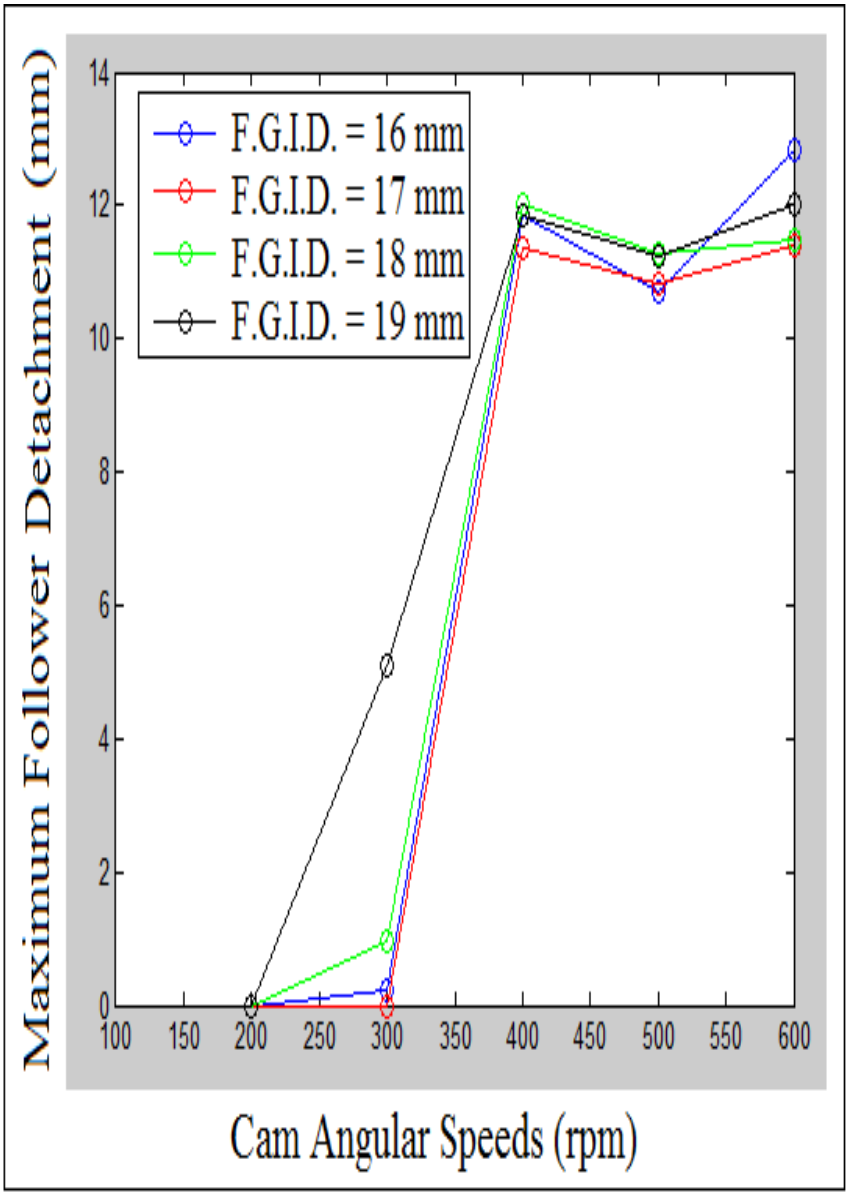

Fig. 28 Maximum follower detachment height against cam angular velocities.

Figures (29) and (30) show the comparison of Fast Fourier Transform (FFT) of the contact force at (F.G.I.D. = 19 mm) and (N = 1000 rpm). The six frequencies peaks with the fundamental frequency is disappeared which means that the nonlinear dynamics of the contact force is non-periodic. It can be noticed that the contact force is approaching zero and the detachment is occurred between the cam and the follower.

ECRTD-UK: https://www.eajournals.org/
ULR: https://doi.org/10.37745/ejmer.2014

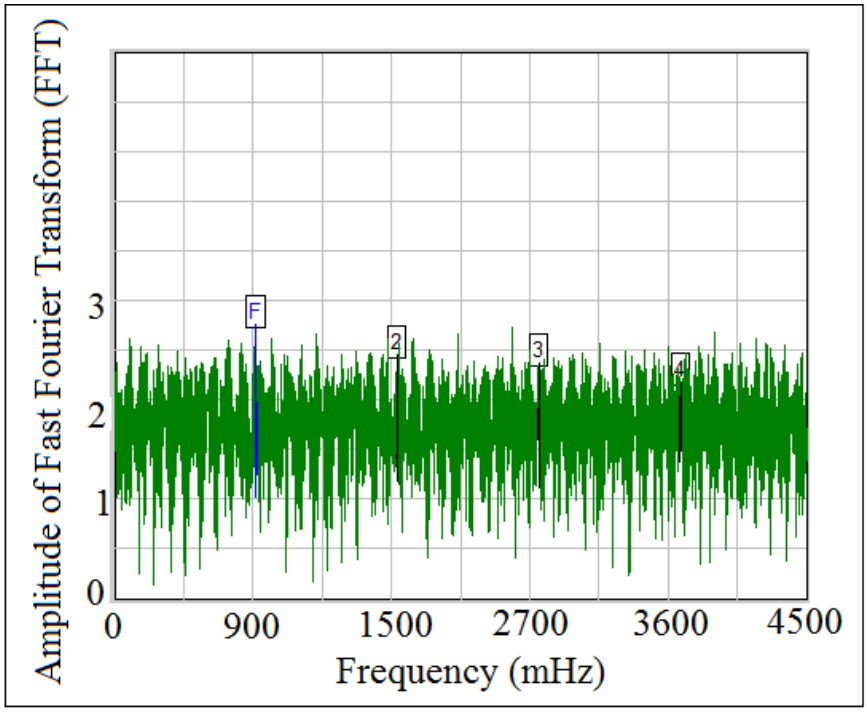

Fig. 29 Power spectrum analysis of experiment test.

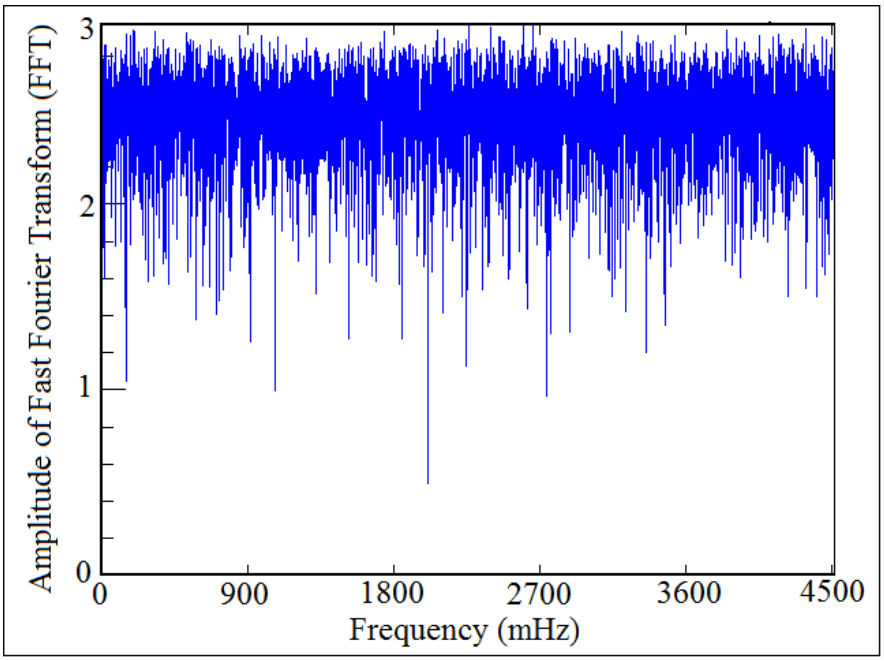

Fig. 30 Power spectrum analysis of numerical simulation.

Figure (31) shows the largest Lyapunov exponent against cam angular velocities at different internal dimensions of the follower guide (F.G.I.D.). The values of largest Lyapunov exponent of

ECRTD-UK: https://www.eajournals.org/
ULR: https://doi.org/10.37745/ejmer.2014

the contact force are increased with the increasing of cam angular velocities. The values of (LLE) for all the systems are the same at N = (200-400 rpm), while (LLE) varies sinusoidal against cam angular velocities at (N = 400-1000 rpm). All the values of (LLE) are positive which gives indication that the contact force is approaching zero and the separation between the cam and the follower has been occurred. SolidWorks is used in the simulation.

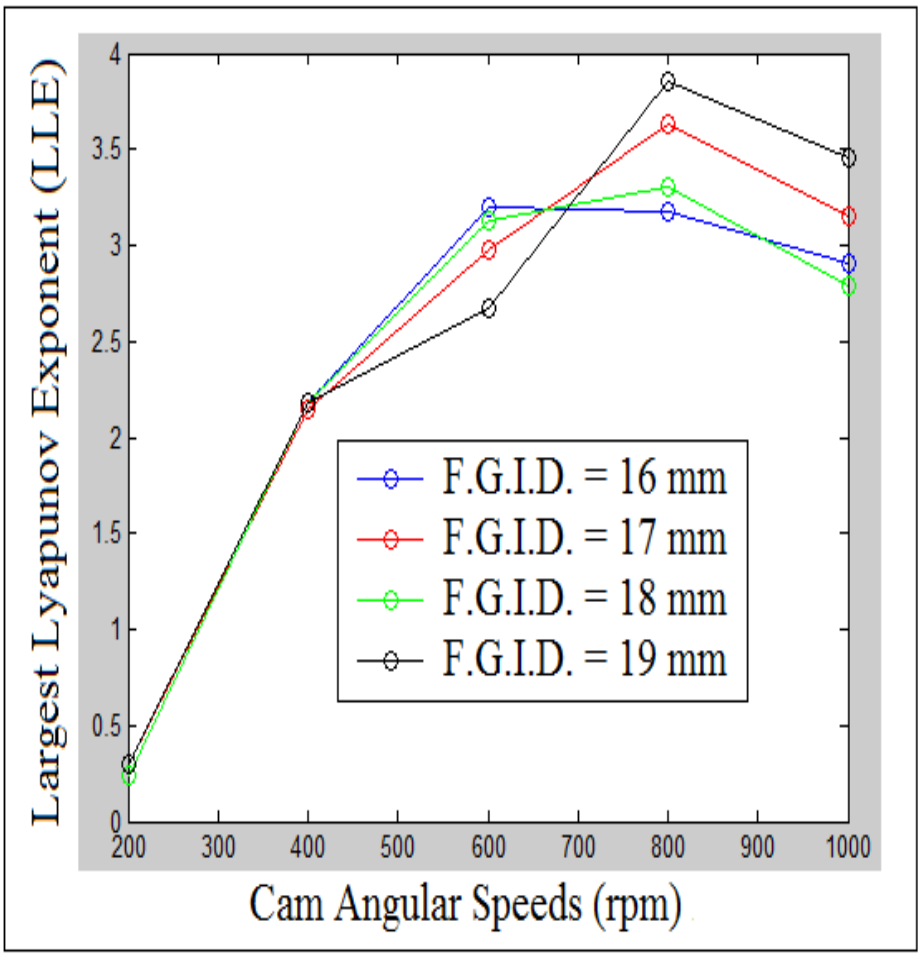

Fig. 31 Largest Lyapunov exponent against cam angular velocities.

Figure (32) shows the rebounding of follower linear displacement against time at different values of coefficient of restitution. The rebounding time of the follower displacement is increased with the increasing of coefficient of restitution. The system without coefficient of restitution is rebounding in less time than the others. SolidWorks is used in the simulation.

ECRTD-UK: https://www.eajournals.org/
ULR: https://doi.org/10.37745/ejmer.2014

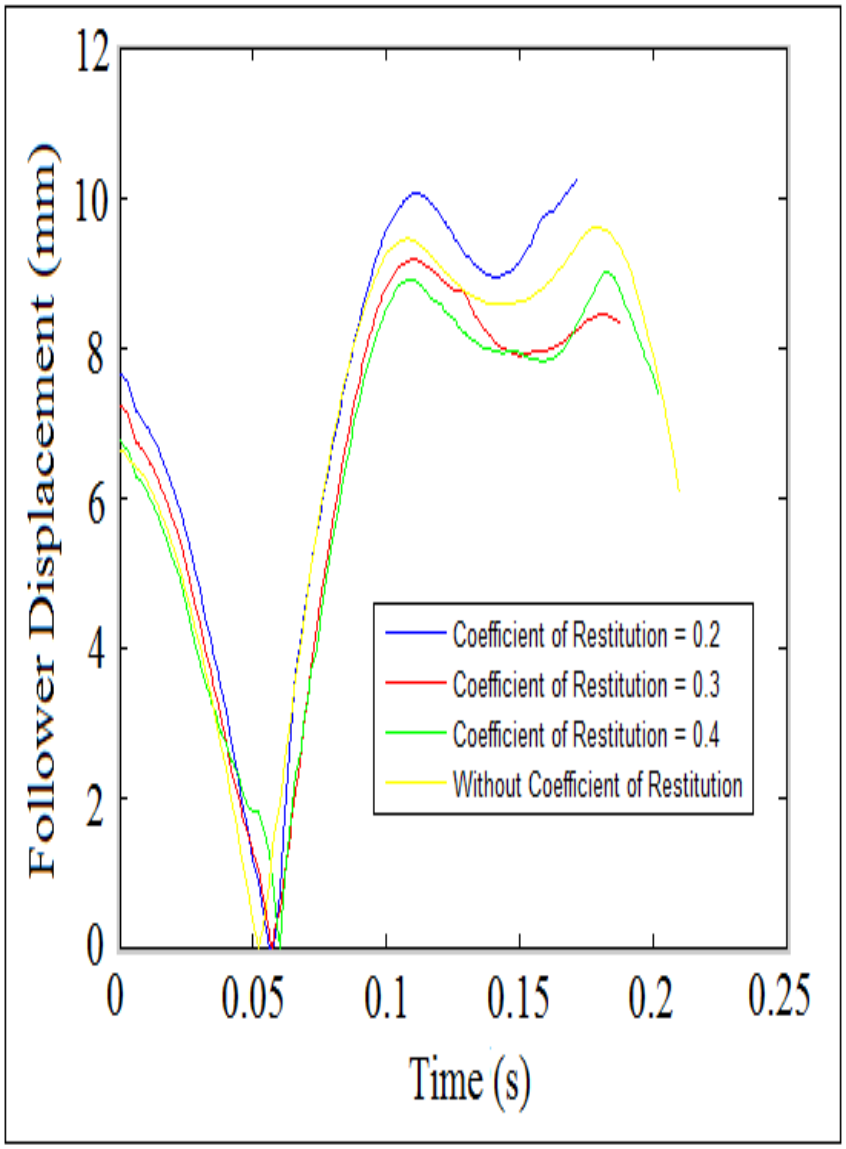

Fig. 32 Follower linear displacement against time at different values of coefficient of restitution.

Figures (33), (34) and (35) show the comparison of follower linear displacement, velocity, and acceleration against time for (F.G.I.D. = 16 mm) and (N = 400 rpm). The experiment set of data of the follower displacement is tracked using OPTOTRAK 30/20 and derived once and twice to determine follower velocity and acceleration respectively. The numerical simulation of the follower displacement, velocity, and acceleration is done using SolidWorks software.

ECRTD-UK: https://www.eajournals.org/
ULR: https://doi.org/10.37745/ejmer.2014

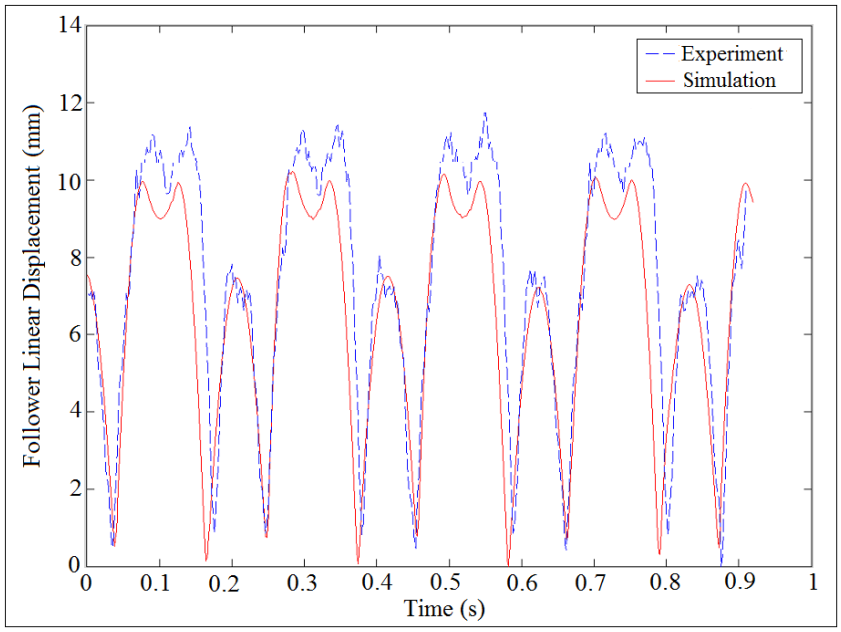

Fig. 33 Comparison of follower linear displacement against time.

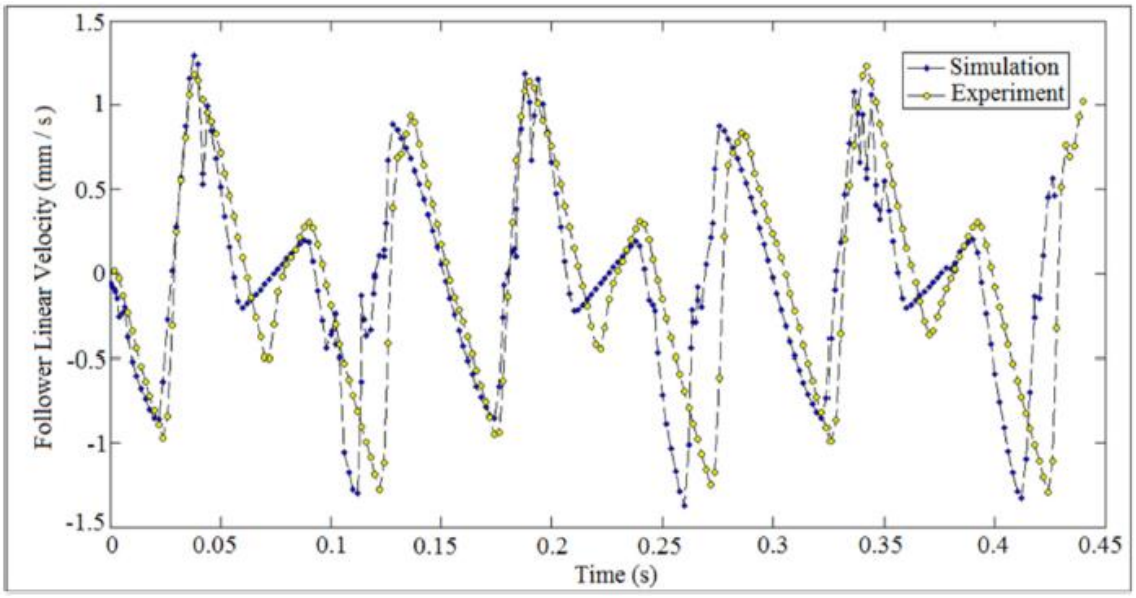

Fig. 34 Comparison of follower linear velocity against time.

ECRTD-UK: https://www.eajournals.org/
ULR: https://doi.org/10.37745/ejmer.2014

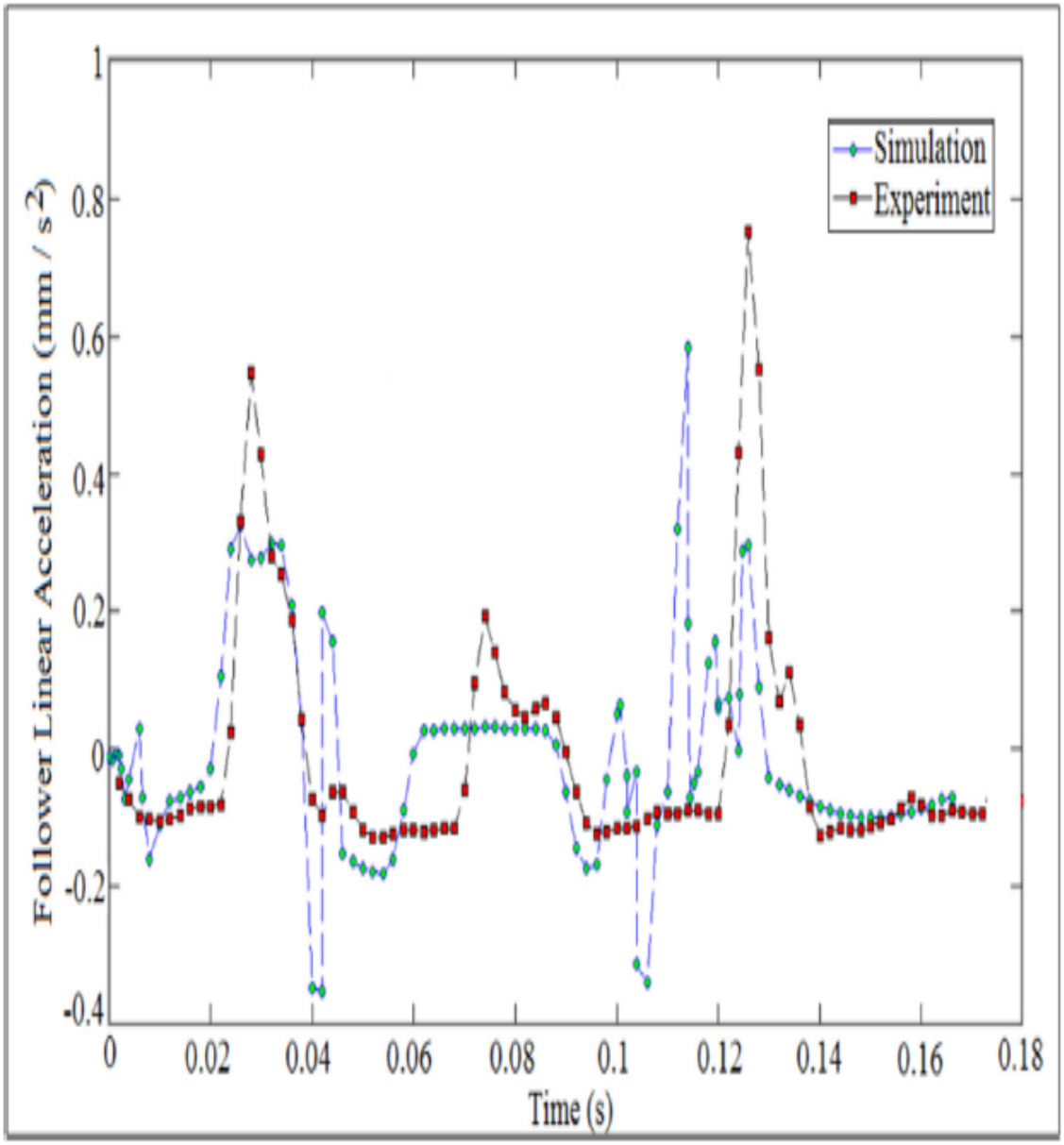

Fig. 35 Comparison of follower linear acceleration against time.

Figures (36) and (37) show the Poincare' maps of the contact force for different internal dimensions of the follower guide (F.G.I.D.) and different cam angular velocities (N). When the black points deceases in Poincare' maps which indicates to non-periodic motion (the follower will detach from the cam). The black points in Poincare' maps are decreased with the increasing of cam angular velocities (N) and internal dimensions of the follower guide (F.G.I.D.). SolidWorks software is used in the simulation.

ECRTD-UK: https://www.eajournals.org/
ULR: https://doi.org/10.37745/ejmer.2014

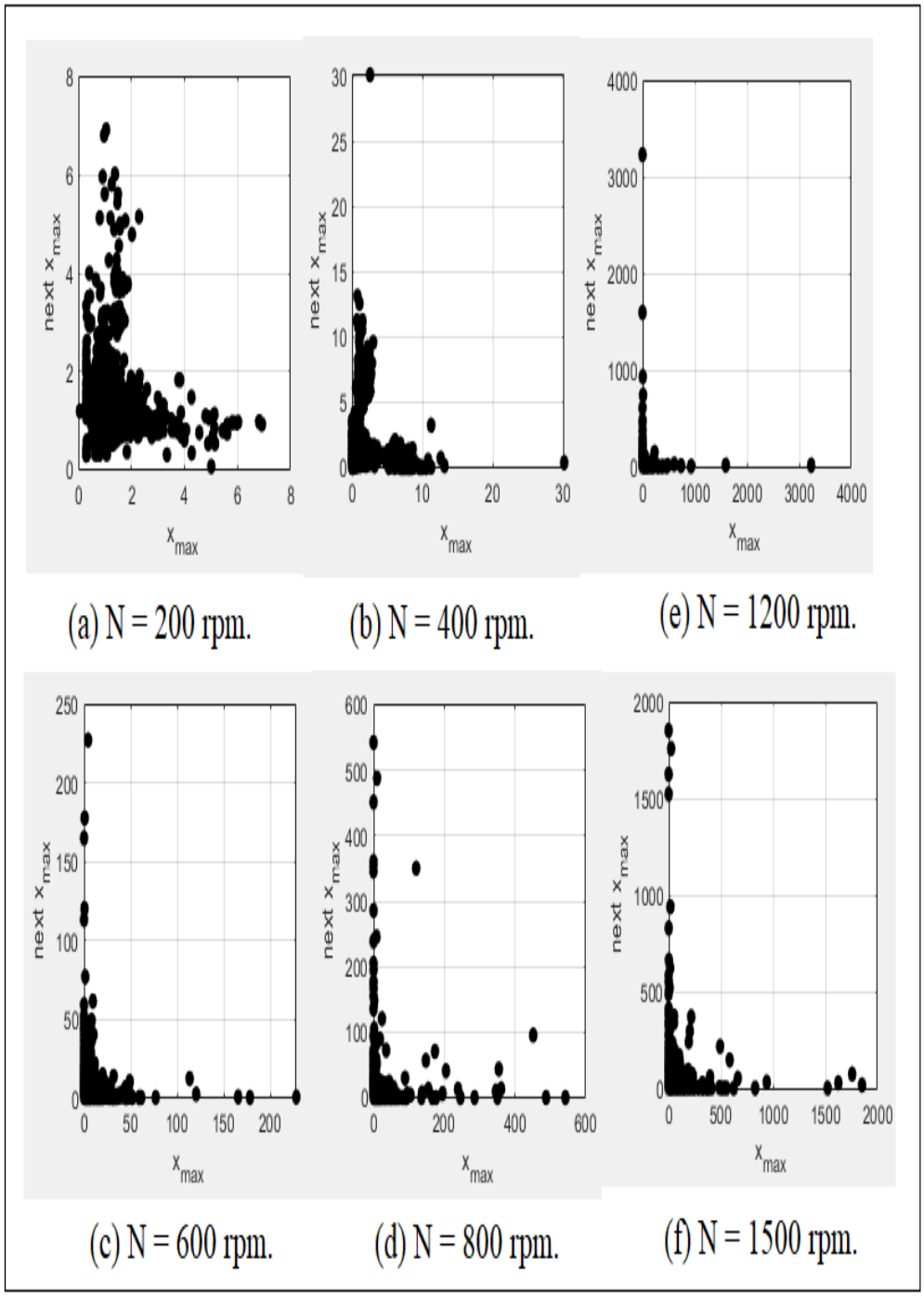

Fig. 36 Poincare' maps for (F.G.I.D. = 17 mm) at different cam angular speeds.

ECRTD-UK: https://www.eajournals.org/
ULR: https://doi.org/10.37745/ejmer.2014

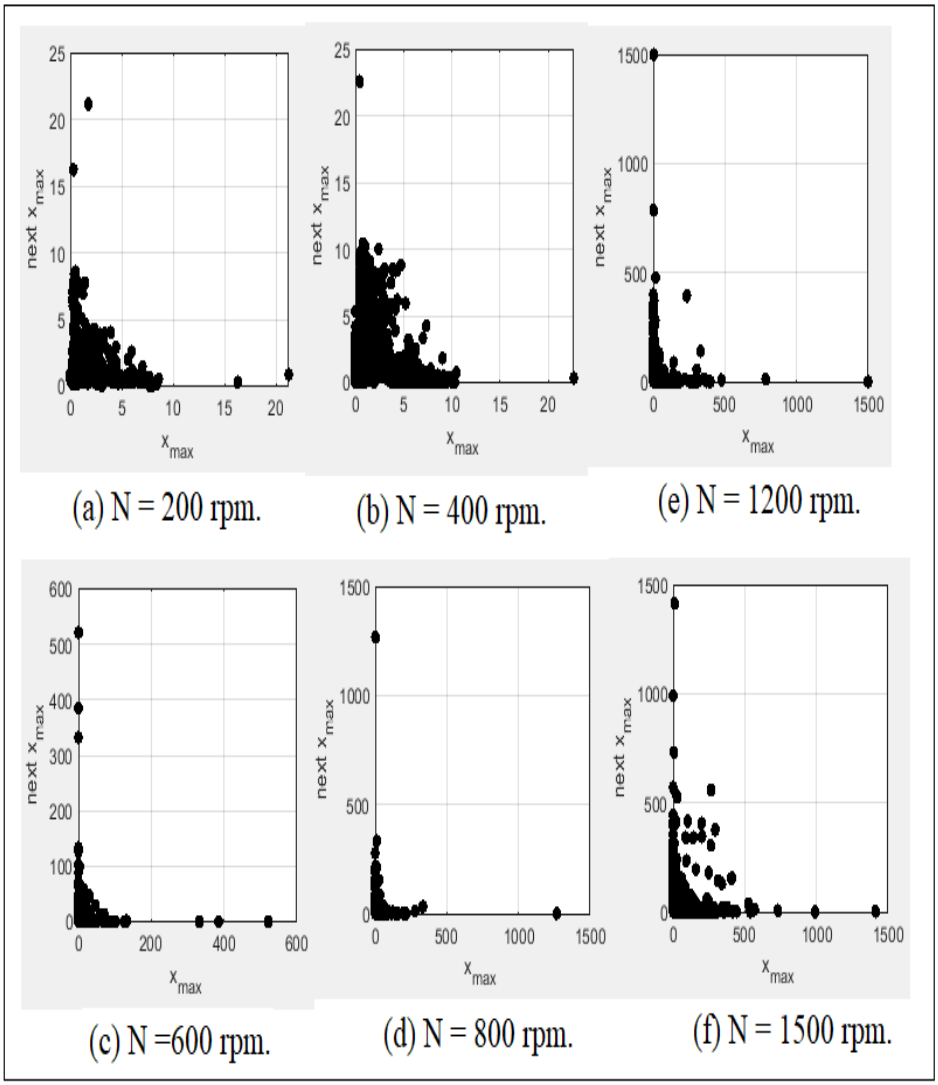

Fig. 37 Poincare' maps for (F.G.I.D. = 19 mm) at different cam angular speeds.

Figure (38) shows the power density function with the dominant frequency of Fast Fourier Transform (FFT) at (F.G.I.D. = 19 mm) and (N = 1000 rpm) for the contact force and follower displacement. The frequencies peaks of power density function of both contact force and follower displacement are disappeared which gives indication to non-periodic motion and the separation will occur between the cam and the follower. The dominant frequency is very intensive for contact force which also gives indication to non-periodic motion. SolidWorks software is used in the simulation.

ECRTD-UK: https://www.eajournals.org/
ULR: https://doi.org/10.37745/ejmer.2014

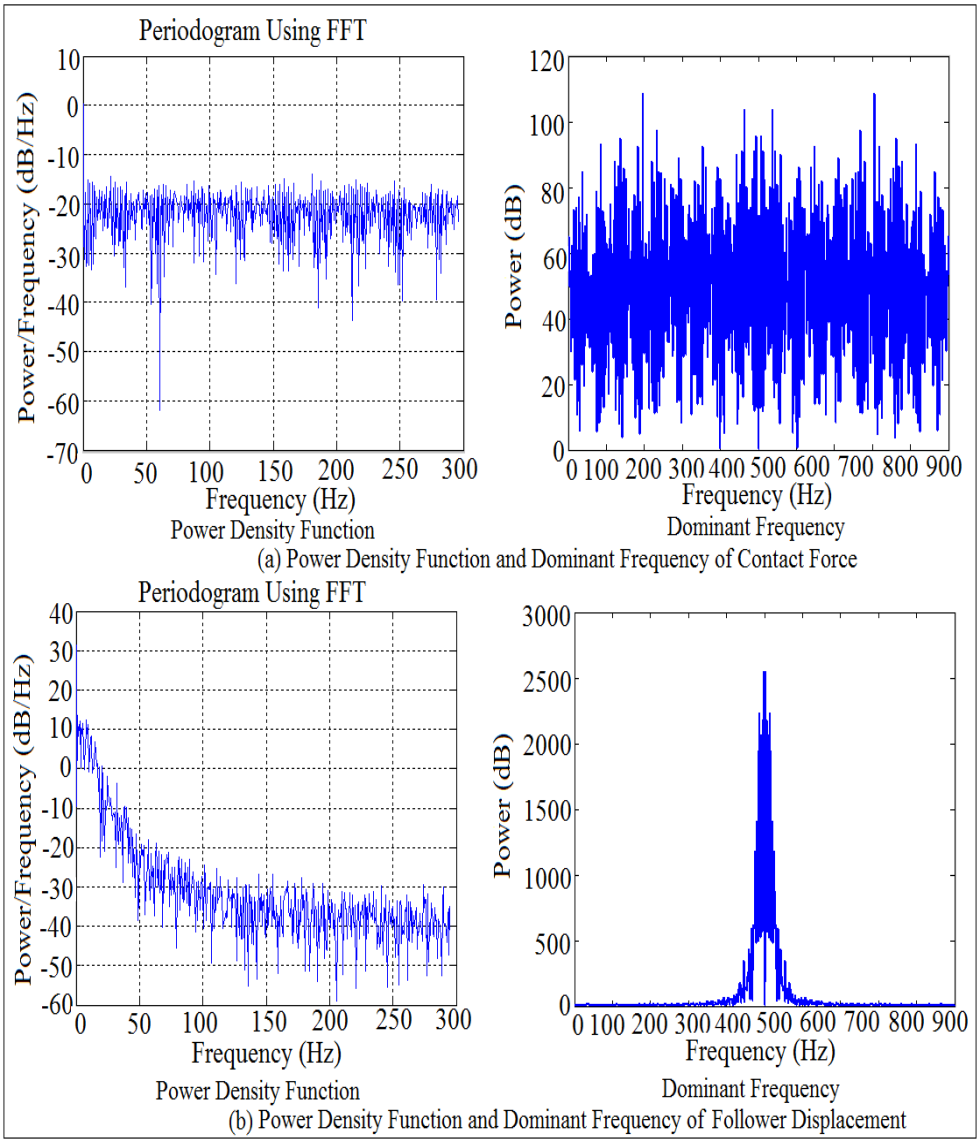

Fig. 38 Power density function and dominant frequency for (F.G.I.D. = 19 mm) and (N = 1000 rpm).

Figure (39) shows the average logarithmic divergence of contact force against time for (F.G.I.D. = 18 mm) and (N = 200 rpm) respectively. The experiment results of Lyapunov exponent is carried out using OPTOTRAK 30/20 device by tracking the follower position and used them as a one column of follower position with time delay and embedding dimension in Wolf algorithm code. The analytic value of Lyapunov exponent is done by calculating one column of the contact force after applying Eqn.(8), while the numerical simulation value of Lyapunov exponent is determined based on one column of the contact force from SolidWorks software.

ECRTD-UK: https://www.eajournals.org/
ULR: https://doi.org/10.37745/ejmer.2014

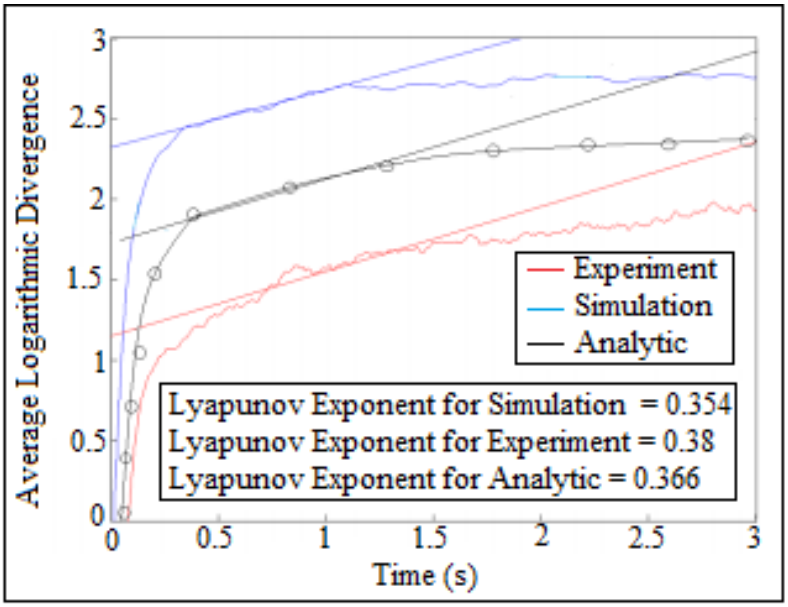

Fig. 39 Average logarithmic divergence against the time for (F.G.I.D. = 18 mm) and (N = 200 rpm).

Figure (40) and (41) show the local Lyapunov exponent against number of samples at (F.G.I.D. = 17 mm and 18 mm) and (N = 600 rpm and 800 rpm) respectively. It can be noticed that the values of Lyapunov exponent is positive which gives indication to non-periodic motion. The values of Lyapunov exponent is taken at their respective equilibrium points. One column of the contact force with the use of time delay and embedding dimension values are used in Wolf algorithm to extract the numerical value of largest Lyapunov exponent parameter. One column of the contact force has been taken from SolidWorks software and used in the dynamic tool of Wolf algorithm program.

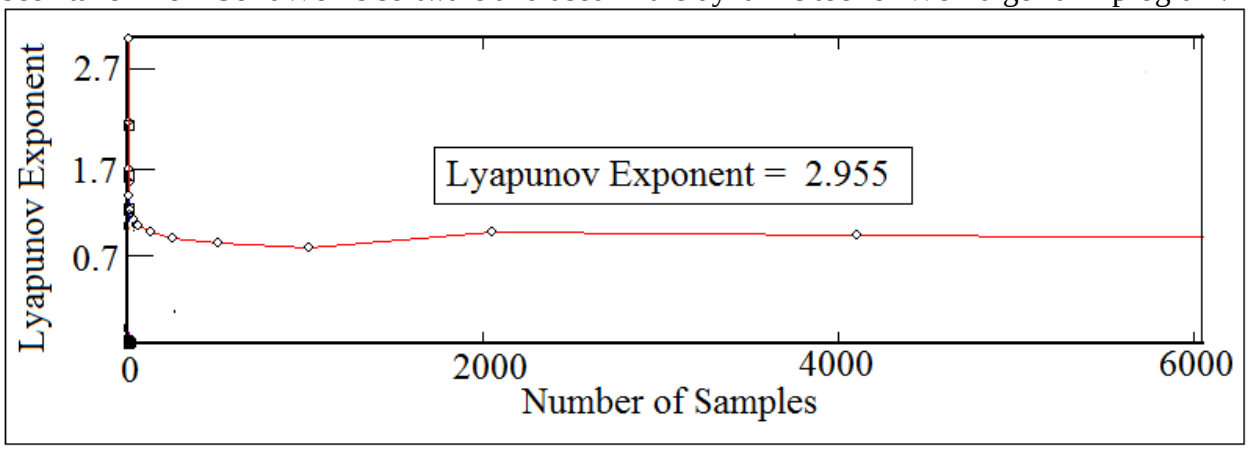

Fig. 40 Local Lyapunov exponent against number of samples for (F.G.I.D. = 17 mm) and (N = 600 rpm).

ECRTD-UK: https://www.eajournals.org/
ULR: https://doi.org/10.37745/ejmer.2014

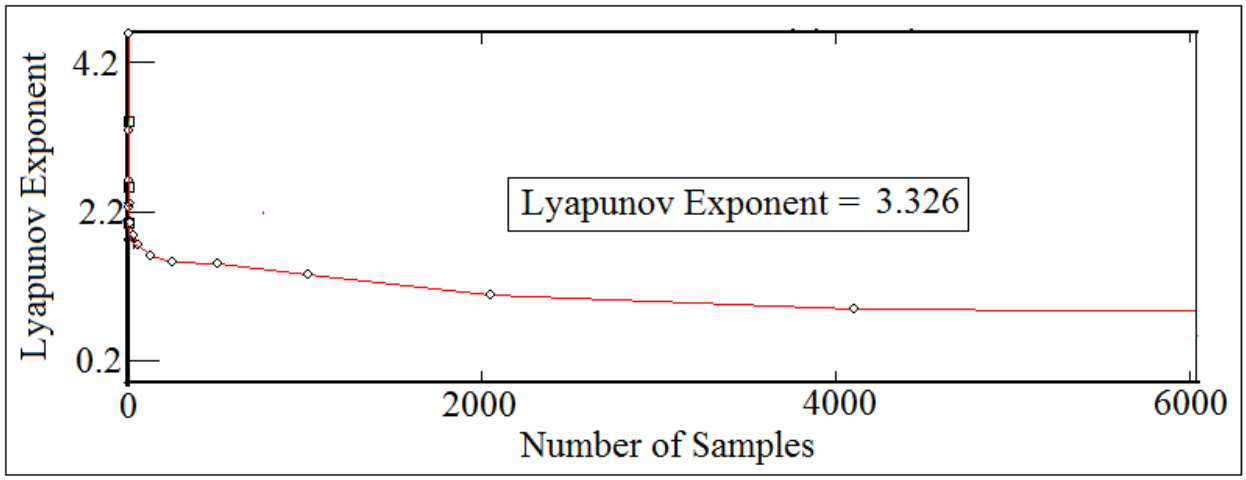

Fig. 41 Local Lyapunov exponent against number of samples for (F.G.I.D. = 18 mm) and (N = 800 rpm).

Figures (42) and (43) show the follower linear displacement against time at (F.G.I.D. = 19 mm) and (N = 200 rpm and 1000 rpm) respectively. In this comparison, two types of friction are used steel greasy and steel dry since both cam and follower are made from steel. The follower displacement of the steel dry friction is bigger than the follower displacement of the steel greasy. The effect of the steel dry friction is very obvious and clear especially at high speeds such as (N = 1000 rpm), while steel greasy and steel dry friction have no effect on the follower displacement at low speeds such as (N = 200 rpm).

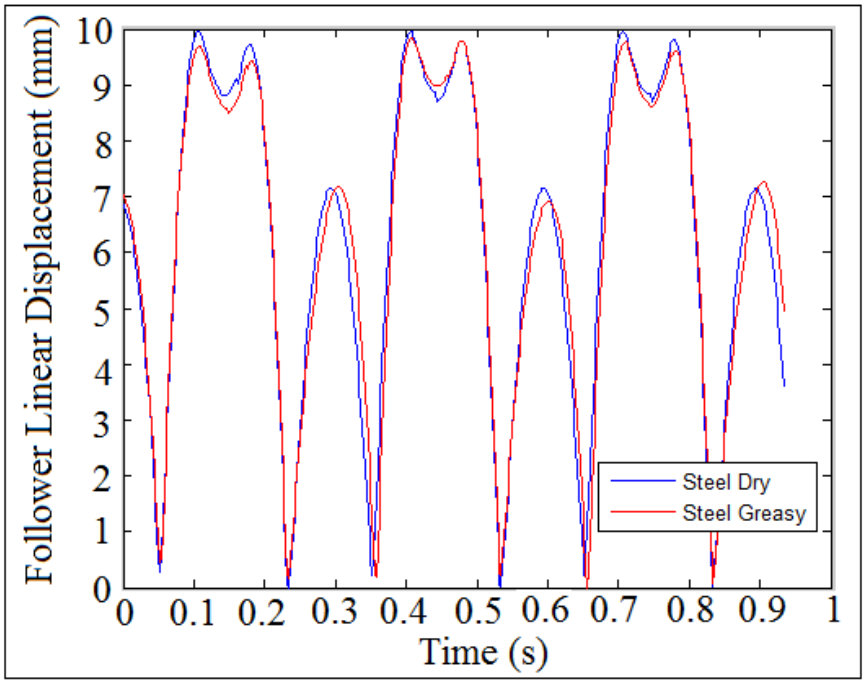

ECRTD-UK: https://www.eajournals.org/
ULR: https://doi.org/10.37745/ejmer.2014

Fig. 42 Follower linear displacement against time at (F.G.I.D. = 19 mm) and (N = 200 rpm) using different types of friction.

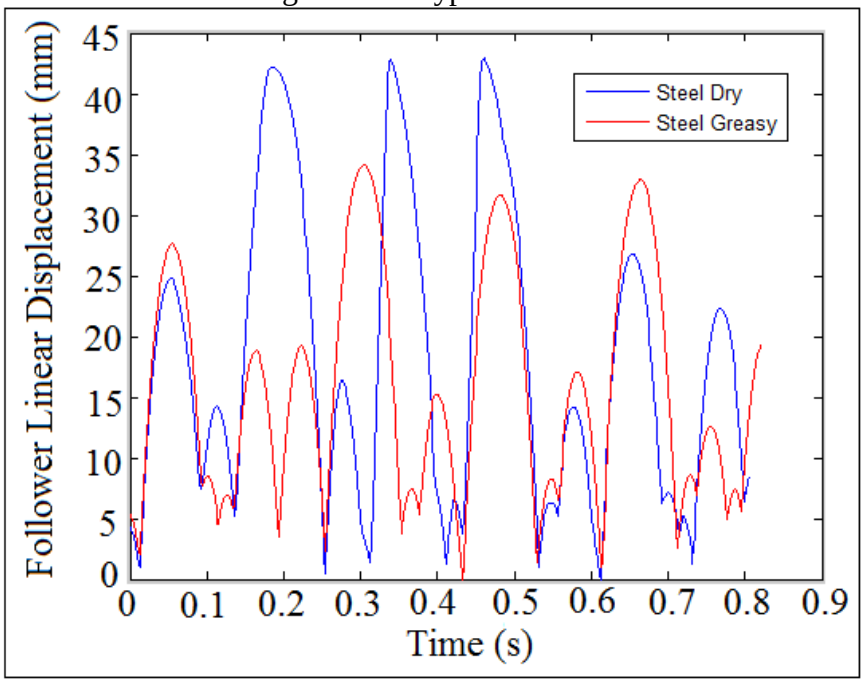

Fig. 43 Follower linear displacement against time at (F.G.I.D. = 19 mm) and (N = 1000 rpm) using different types of friction.

CONCLUSIONS

This study is analyzed and discussed the largest Lyapunov exponent parameter of the contact force due to high speeds of the cam. All the values of largest Lyapunov exponent are positive which means that there will be a detachment between the cam and the follower (contact force is approaching zero). The value of contact force has declined with the increasing of cam angular velocities (N) and internal dimension of the follower guide (F.G.I.D.). The system with (F.G.I.D. = 18 mm) and (N =1500 rpm) has a minimum value of contact force. The detachment height of the follower is in a minimum value at (N = 200-300 rpm) for (F.G.I.D. = 16, 17, and 18 mm). The black points in Poincare' maps are decreased with the increasing of cam angular velocities (N) and internal dimensions of the follower guide (F.G.I.D.). The broken lines in the upper and lower surfaces in the phase-plane diagram is increased with the increasing of coefficient of restitution values. The variation of the follower movement is increased with the increasing of coefficient of restitution values.

Recommendations of the Future Work

The recommendation of the future work is as below:
(1) Genetic Algorithm Optimization of Contact Force in Cam-Follower System Using Lyapunov Exponent Conception.

ECRTD-UK: https://www.eajournals.org/
ULR: https://doi.org/10.37745/ejmer.2014

(2) Nonlinear Dynamics Detection of Contact Force Using Phase-Plane Diagram and Poincare' Maps.

Conflict of Interest

The author declares that he has no conflict of interest and there is no institution was funding and supporting this research.

Data Availability Statements

The data that support the findings of this study are available from the corresponding author upon reasonable request.

References

[1] Sundar S, Dreyer JT, Singh R (2013) Rotational sliding contact dynamics in a non-linear cam-follower system as excited by a periodic motion. J Vib Acoust 332(18):4280-4295, Elsevier Publisher.
[2] Alzate R, Di Bernardo M, Montanaro U, Santini S (2007) Experimental and numerical verification of bifurcations and chaos in cam-follower impacting systems. J Nonlinear Dyn 50(3):409-429, Springer Publisher.
[3] Ciulli E, Fazzolari F, Pugliese G (2020) Contact Force Measurements in Cam and Follower Lubricated Contacts. Front. J Front Mech Eng 6:601410, Springer Publisher.
[4] Yousuf LS (2020) Deflection calculation of cam profile due to a Hertzian contact pressure. J Mech 37:149-160, Oxford Academic Publisher.
[5] Yousuf LS, Dabool YKH (2020) Numerical Simulation of Dynamic Bending Deflection of a Disc Cam Profile With Roller Follower System. IMECE Int Mech Eng Congress Exposition Conf 84270:V001T16A001, ASME Publisher.
[6] Yousuf LS, Hadi NH (2021) Contact Stress Distribution of a Pear Cam Profile with Roller Follower Mechanism. Chin J Mech Eng 34(1):1-14, Springer Publisher.
[7] Pugliese G, Ciulli E, Fazzolari F (2019) Experimental aspects of a cam-follower contact. IFToMM World Congress Mech Mach Sci Conf 3815-3824, Springer Publisher.
[8] Yang Y-F, Lu Y, Jiang T-D, Lu N (2016) Modeling and nonlinear response of the cam-follower oblique-impact system. Disc Dyn Nat Soc 2016, Hindawi Publisher.
[9] Yousuf LS (2019) Experimental and simulation investigation of nonlinear dynamic behavior of a polydyne cam and roller follower mechanism. J Mech Syst Signal Process 116:293-309, Elsevier Publisher.
[10] Yousuf LS, Dabool YKH (2020) Insight Into the Non Periodic Motion of the Knife Follower With a Polydyne Cam Mechanism. IDETC-CIE Int Des Eng Tech Conf Comp Info Eng Conf 83914:V002T02A037, ASME Publisher.
[11] Yousuf LS, Marghitu DB (2020) Lyapunov Exponent for a Globoidal Cam With a Roller Follower Mechanism Using Wolf Algorithm. IMECE Int Mech Eng Congress Exposition Conf 84553:V07BT07A007, ASME Publisher.
[12] Yousuf LS, Marghitu DB (2020) Nonlinear dynamics behavior of cam-follower system using concave curvatures profile. J Adv Mech Eng 12(9):1687814020945920, Sage Publisher.

[13] Shakoor MM (2006) Fatigue life investigation for cams with translating roller-follower and translating flat-face follower systems. Ph.D. Dissertation, Iowa State University Publisher.

[14] Hamza F, Abderazek H, Lakhdar S, Ferhat D, Yıldız AR (2018) Optimum design of cam-roller follower mechanism using a new evolutionary algorithm. Int J Adv Manuf Syst, 99(5): 1267–1282, Springer Publisher.
[15] Planchard D (2015) SolidWorks 2016 Reference Guide: A comprehensive reference guide with over 250 standalone tutorials. Sdc Publisher.
[16] Yousuf LS, Marghitu DB (2020) Analytic and numerical results of a disc cam bending with a roller follower. SN J Appl Sci, 2(10): 1–15, Springer Publisher.
[17] Yousuf LS, Marghitu DB (2017) Experimental and simulation results of a cam and a flat-faced follower mechanism. J Comput Nonlinear Dyn, 12(6), ASME Publisher.
[18] Yousuf LS (2020) Investigation of chaos in a polydyne cam with flat-faced follower mechanism. J King Saud Univ Eng Sci, Elsevier Publisher.
[19] Yousuf LS, Marghitu DB (2017) Non-linear dynamic analysis of a cam with flat-faced follower linkage mechanism. IMECE Int Mech Eng Congress Exposition Conf,58370:V04AT05A051, ASME Publisher.
[20] Parlitz U (2016) Estimating lyapunov exponents from time series. Chaos Detection and Predictability,1-34, Springer Publisher.
[21] Yousuf LS, Marghitu DB (2016) Experimental and simulation of a cam and translated roller follower over a range of speeds, IMECE Int Mech Eng Congress Exposition Conf, 50541:V04AT05A057, ASME Publisher.
[22] Stoica P, Moses RL (2005) Spectral analysis of signals, ICSTCC Int Conf Syst Theory Control Comput , Pearson Prentice Hall Upper Saddle River Publisher.
[23] Abu-Mahfouz I (2005) Experimental investigation of non-linear behavior of a cam-follower mechanism, SEM Annual Conf Expo Exp Appl Mech, 1930-1936, SEM Publisher.
[24] Rothbart HA (2004) Cam design handbook, McGraw-Hill Education Publisher.

Nomenclatures

F.G.I.D.: Follower guides internal dimensions, mm.

N: Cam angular velocity, rpm.

Ω: Angular velocity of the cam, Rad/s.

ω: Natural frequency of the follower stem, Rad/s.

x_H: Homogeneous solution of the follower movement, mm.

x_P: Particular solution of the follower movement, mm.

ECRTD-UK: https://www.eajournals.org/
ULR: https://doi.org/10.37745/ejmer.2014

x: General solution of the follower movement, mm.

k: Spring stiffness which locates at the end of the follower stem, N/mm.

c: Viscous damping coefficient which locates at the end of the follower stem, N.s/mm.

x, ẋ, ẍ: Linear displacement, velocity, and acceleration of the roller follower, mm, mm/s, mm/s^2.

m: Mass of the follower, kg.

k_1: Spring Stiffness which locates between the follower and the installation table, N/mm.

Δ: Preload extension, mm.

P_C: Contact force between the cam and the follower, N.

Ø: Pressure angle, degree.

D: Average displacement between trajectories at (t=0).

d(t): Rate of change in the distance between nearest neighbors.

$d_j(i)$: Distance between the j^{th} pair at (i) nearest neighbors, mm.

t: Single time series, s.

y(i): Curve fitting of least square method for the follower displacement data.

Δ(t): Discrete time steps, s.

λ: Lyapunov exponent.

AMI : Average mutual information.

GFNN : Global False Nearest Neighbors.

LLE: Largest Lyapunov exponent parameter.

ECRTD-UK: https://www.eajournals.org/
ULR: https://doi.org/10.37745/ejmer.2014